

RESEARCH

Open Access



Modulating tumor infiltrating myeloid cells to enhance bispecific antibody-driven T cell infiltration and anti-tumor response

Jeong A. Park[†], Linlin Wang[†] and Nai-Kong V. Cheung^{* ID}

Abstract

Background: Tumor microenvironment (TME) is a dynamic cellular milieu to promote tumor angiogenesis, growth, proliferation, and metastasis, while derailing the host anti-tumor response. TME impedes bispecific antibody (BsAb) or chimeric antigen receptor (CAR)-driven T cells infiltration, survival, and cytotoxic efficacy. Modulating tumor infiltrating myeloid cells (TIMs) could potentially improve the efficacy of BsAb.

Methods: We evaluated the effects of TIM modulation on BsAb-driven T cell infiltration into tumors, their persistence, and in vivo anti-tumor response. Anti-GD2 BsAb and anti-HER2 BsAb built on IgG-[L]-scFv platform were tested against human cancer xenografts in BALB-*Rag2*^{-/-}IL-2R- γ -KO (BRG) mice. Depleting antibodies specific for polymorphonuclear myeloid-derived suppressor cell (PMN-MDSC), monocytic MDSC (M-MDSC), and tumor associated macrophage (TAM) were used to study the role of each TIM component. Dexamethasone, an established anti-inflammatory agent, was tested for its effect on TIMs.

Results: BsAb-driven T cells recruited myeloid cells into human tumor xenografts. Each TIM targeting therapy depleted cells of interest in blood and in tumors. Depletion of PMN-MDSCs, M-MDSCs, and particularly TAMs was associated with enhanced T cell infiltration into tumors, significantly improving tumor control and survival in multiple cancer xenograft models. Dexamethasone premedication depleted monocytes in circulation and TAMs in tumors, enhanced BsAb-driven T cell infiltration, and anti-tumor response with survival benefit.

Conclusion: Reducing TIMs markedly enhanced anti-tumor effects of BsAb-based T cell immunotherapy by improving intratumoral T cell infiltration and persistence. TAM depletion was more effective than PMN- or M-MDSCs depletion at boosting the anti-tumor response of T cell engaging BsAb.

Keywords: Bispecific antibody, Dexamethasone, Disialogangliosides, Ex vivo bispecific antibody armed T-cells (EATs), Human epidermal growth factor receptor 2 (HER2), Immunotherapy, Myeloid-derived suppressor cell, T cell, Tumor infiltrating myeloid cell, Tumor microenvironment, Tumor-associated macrophage

Introduction

T cell-based immunotherapy has emerged as one of the most promising therapeutic modalities for refractory or relapsed cancers. Yet, major hurdles still remain. Besides

their inability to reach and penetrate solid tumors, T cells tend to be exhausted or inhibited by immunosuppressive tumor microenvironment (TME) [1]. TME plays a key role in tumor development, growth, and metastasis [2], and the reciprocal interactions between cancer cells and TME promote cancer cell stemness and induce metabolic derangement by creating hypoxic and acidic environment [3]. The immune-hostile TME increases cancer-associated neutrophils and recruits myeloid-derived suppressor

*Correspondence: cheungn@mskcc.org

[†]Jeong A. Park and Linlin Wang are co first authors

Department of Pediatrics, Memorial Sloan Kettering Cancer Center, 1275 York Avenue, New York, NY 10065, USA



© The Author(s) 2021. **Open Access** This article is licensed under a Creative Commons Attribution 4.0 International License, which permits use, sharing, adaptation, distribution and reproduction in any medium or format, as long as you give appropriate credit to the original author(s) and the source, provide a link to the Creative Commons licence, and indicate if changes were made. The images or other third party material in this article are included in the article's Creative Commons licence, unless indicated otherwise in a credit line to the material. If material is not included in the article's Creative Commons licence and your intended use is not permitted by statutory regulation or exceeds the permitted use, you will need to obtain permission directly from the copyright holder. To view a copy of this licence, visit <http://creativecommons.org/licenses/by/4.0/>. The Creative Commons Public Domain Dedication waiver (<http://creativecommons.org/publicdomain/zero/1.0/>) applies to the data made available in this article, unless otherwise stated in a credit line to the data.

cells (MDSCs) and M2-polarized tumor associated macrophages (TAMs) [4, 5]. These tumor-infiltrating myeloid cells (TIMs) constitute a heterogeneous population of cells marked by diversity, plasticity, and immaturity and function as potent mediators of immune suppression, tumor angiogenesis, and tumor cell metastases [6–8]. In murine tumor models, TIMs are commonly classified as either ‘pro-tumoral’ M2 TAMs or MDSCs. MDSCs are further subdivided into 2 major groups: CD11b⁺Ly6G⁺Ly6C^{lo} polymorphonuclear MDSC (PMN-MDSC) and CD11b⁺Ly6G⁻Ly6C^{hi} monocytic MDSC (M-MDSC) [9–14]. MDSCs inhibit T cell metabolism by hoarding key amino acids [15–17], modulate T cell homing by cleaving L-selectin [4, 18], and prevent T cell activation through PD-L1 upregulation especially when hypoxic [19]. Immunosuppressive M2 TAMs promote T cell anergy via increased nitric oxide (NO) and decreased arginine under hypoxic conditions [20]. Modulating these TIMs has the potential to improve anti-tumor response of T cell-based cancer immunotherapies.

We previously demonstrated that the IgG-[L]-scFv-formatted T cell engaging bispecific antibody (T-BsAb) was highly effective in driving human T cells into human tumor xenografts [21]. Here, we explore the effects of myeloid cell depleting strategies targeting TAM, PMN-MDSC, or M-MDSC, as well as dexamethasone, on T-BsAb mediated immunotherapy, with specific emphasis on T cell infiltration into tumors and in vivo anti-tumor activity.

Methods

Construction and expression of BsAbs

The construction of the GD2-BsAb was described previously [22]. For each BsAb, scFv of huOKT3 was fused to the C-terminus of the light chain of human IgG1 via a C-terminal (G₄S)₃ linker [23]. N297A and K322A on Fc were generated with site-directed mutagenesis via primer extension in polymerase chain reactions [24]. The nucleotide sequence encoding each BsAb was synthesized by GenScript and was subcloned into a mammalian expression vector. BsAb was produced using Expi293TM expression system (Thermo Fisher Scientific RRID:CVCL_D615) separately. Antibodies were purified with protein A affinity column chromatography. The purity of these antibodies was evaluated by size-exclusion high-performance liquid chromatography (SE-HPLC).

Cell lines

Representative melanoma cell line M14 (UCLA-SO-M14, NCI-DTP Cat# M14, RRID:CVCL_1395), osteosarcoma cell line 143B (ATCC Cat# CRL-8303, RRID:CVCL_2270) and small cell lung cancer (SCLC) cell line NCI-N417 (ATCC Cat# CRL-5809, RRID:CVCL_1602) were used.

All the cell lines used were authenticated by short tandem repeat profiling with the PowerPlex 1.2 System (Promega, Cat# DC8942), and periodically tested for mycoplasma infection using MycoAlertTM PLUS Mycoplasma Detection Kit (Lonza, Cat# LT07-318). The cells were cultured in RPMI1640 (Sigma) supplemented with 10% heat-inactivated fetal bovine serum (FBS, Life Technologies) at 37 °C in a 5% CO₂ humidified incubator. The luciferase-labeled osteosarcoma cell line 143BLuc and melanoma cell line M14Luc were generated by retroviral infection with an SFG-GF Luc vector.

BsAb treatment and depleting antibodies

10 µg of GD2-BsAb was given intravenously with 2×10^7 of effector T cells or as ex vivo GD2-BsAb armed T cells (GD2-EATs). Ex vivo BsAb armed T cells (EATs) were generated as follows: T cells isolated from peripheral blood mononuclear cells (PBMCs) were activated with CD3/CD28 Dynabeads (GibcoTM, Cat#11132D) for 7 to 14 days in the presence of 30 IU/mL of IL-2. 2×10^7 of activated T cells were armed with 10 µg of each BsAb for 20 min at room temperature [21]. After incubation, the T cells were washed with PBS twice. EATs were tested for cell surface density of BsAb using idiotype antibody and in vitro cytotoxicity against target antigens. Activated T cells or EATs were injected intravenously with 1000 IU of IL-2 given subcutaneously. For depletion of tumor infiltrating myeloid cells, 100 µg of anti-mouse GR1((Bio X Cell Cat# BE0320, RRID:AB_2819047), 100 µg of anti-mouse Ly6G (Bio X Cell Cat# BE0075-1, RRID:AB_1107721), 100 µg of anti-mouse Ly6C antibody (Bio X Cell Cat# BE0203, RRID:AB_2687696), 100 µg of anti-mouse CSF-1R (CD115) antibody (Bio X Cell Cat# BE0213, RRID:AB_2687699), or 10µL of clodronate liposome (Liposoma B.V., Cat#SKU-C005) was given iv one day before, and dexamethasone sodium phosphate were given ip one hour before, each BsAb or EAT injection.

Anti-tumor effect in human tumor xenografts

All animal procedures were performed in compliance with Memorial Sloan Kettering Cancer Center’s institutional Animal Care and Use Committee (IACUC) guidelines. In vivo anti-tumor response was evaluated using cancer cell line- or patient-derived xenografts (CDXs or PDXs). Target antigen (+) patient-derived xenograft (PDX) was established from fresh surgical specimens with MSKCC IRB approval. Tumor cells suspended in Matrigel (Corning Corp, Cat#354234) or PDXs were implanted in the right flank of 6–10-week-old BALB-Rag2-/-IL-2R-γc-KO (BRG) mice (Taconic Biosciences). To avoid biological variables, only female mice were used for in vivo experiments. Treatment was initiated after tumors were established, average tumor volume of 100

mm³ when measured using TM900 scanner (Piera, Brussels, BE). Before treatment, mice with small tumors (<50 mm³) or infection signs were excluded from the experiments, and the included mice were randomly assigned to each group. Tumor growth curves and overall survival was analyzed, and the overall survival was defined as the time from start of treatment to when tumor volume reached 2000 mm³. To define the well-being of mice, CBC analyses, changes in body weight, behavior and physical appearance were monitored. All animal experiments were repeated twice more with different donor's T cells to ensure that our results were reliable.

T cell transduction

T cells isolated from peripheral blood (PB) were stimulated with Dynabeads™ Human T-Activating CD3/CD28 beads (Gibco™, Cat#11132D) for 24 h. T cells were transduced with retroviral constructs containing tdTomato and click beetle red luciferase in RetroNectin-coated 6-well plates in the presence of IL-2 (100 IU/ml) and protamine sulfate (4 µg/mL). Transduced T cells were cultured for 8 days before being used in animal experiments.

Bioluminescence imaging

Mice were anesthetized and imaged after intravenous injection of 3 mg of D-luciferin (Gold Biotechnology, Cat# LUCK-100) on different days post T cell injection. Images were acquired using IVIS Spectrum CT In Vivo Imaging System (Caliper Life Sciences). Bioluminescence images were overlaid onto photographs, and regions of interest (ROI) were drawn based on the location and contour of tumor using Living image 2.60 (Xenogen) to quantify bioluminescence emission (BLI, photon flux/sec).

Flow cytometry analysis and cytokine assay

For blood and tumor samples from mice, the following antibodies were purchased from BioLegend: anti-human CD45-APC (BioLegend Cat# 304011, RRID:AB_314399), anti-human CD45-Brilliant Violet 421™ (BioLegend Cat# 304032, RRID:AB_2561357), anti-human CD4-APC (BioLegend Cat# 300514, RRID:AB_314082), anti-human CD4-PE/Cyanine7 (BioLegend Cat# 300512, RRID:AB_314080), anti-human CD8-FITC (BioLegend Cat# 980908, RRID:AB_2888883), anti-human CD8-Brilliant Violet785™ (BioLegend Cat# 344739, RRID:AB_2566201), anti-mouse CD45-APC (BioLegend Cat# 103111, RRID:AB_312976), anti-mouse CD45-Brilliant Violet 711™ (BioLegend Cat# 103147, RRID:AB_2564383), anti-mouse/human CD11b-Brilliant Violet 570™ (BioLegend Cat# 101233, RRID:AB_10896949), anti-mouse/human CD11b-PE

(BioLegend Cat# 101208, RRID:AB_312791), anti-mouse/human CD11b-PE/Cyanine7 (BioLegend Cat# 101215, RRID:AB_312798), anti-mouse Ly6G-FITC (BioLegend Cat# 127606, RRID:AB_1236494), anti-mouse Ly6G-PerCP/Cyanine5.5 (BioLegend Cat# 127616, RRID:AB_1877271), anti-mouse Ly-6C-PerCP/Cyanine5.5 (BioLegend Cat# 128012, RRID:AB_1659241), anti-mouse F4/80-PE/Cyanine7 (BioLegend Cat# 123114, RRID:AB_893478), anti-mouse F4/80-PE (BioLegend Cat# 123110, RRID:AB_893486).

Immunohistochemistry and immunofluorescence staining

Immunohistochemistry (IHC) and immunofluorescence (IF) staining were performed at the MSK Molecular Cytology Core Facility using Discovery XT processor (Ventana Medical Systems) as previously described [22]. Tumor samples were fixed and embedded in paraffin. Anti-human CD45, anti-human CD3, anti-human CD4, anti-human CD8, anti-human FoxP3, anti-mouse CD45, anti-mouse CD11b, anti-mouse CD68, and anti-mouse IBA1 antibodies were used, which were followed by biotinylated secondary antibody. The detection was performed using a DAB detection kit (Ventana Medical Systems) or Alexa Fluor™ 488 or 568 Tyramide Reagent (Invitrogen). IHC images were captured from tumor sections using a Nikon ECLIPSE Ni-U microscope and NIS-Elements 4.0 imaging software. IF images were captured using Leica Inverted Confocal SP8 and processed with Imaris (Bitplane). Antigen positive cells were counted with Qupath 0.1.2.

Positive pixel count analysis

IHC slides were scanned (Aperio ScanScope XT) and analyzed by comparing positive pixel counts (Aperio Technologies). For analyzing tumor infiltrating lymphocytes, the largest area of intact tumor tissue was included, and oblique sections were avoided. Each slide was visually inspected to ensure specificity and sensitivity of antibody staining. After positive pixel count analysis was run, analyzed slides were examined to confirm that positively identified pixels were consistent with lymphocyte staining and not background staining. Percentages were calculated as the total number of positive pixels divided by the total number of pixels (% positive pixels/total pixels).

Statistical analysis

In vivo anti-tumor effect was compared by area under curve (AUC) and survival curve analyses. TILs were quantified using AUC of BLIs. Differences between samples indicated in the figures were tested for statistical significance by two-tailed Student's t-test for two sets of data while one-way ANOVA with Tukey's post hoc test was used to among three or more sets of data.

(See figure on next page.)

Fig. 1 The effects of granulocyte depletion on bispecific antibody (BsAb) directed T cell immunotherapy. **A** Neuroblastoma patient-derived xenografts (PDXs) treated with GD2-BsAb armed T cells (GD2-EATs) or unarmed T cells were compared with untreated tumors. All tumors were harvested on day 10 after the start of treatment. Immunohistochemical (IHC) staining of the tumor sections by anti-human CD3 antibody ($\times 10$), anti-human CD4 antibody ($\times 10$), anti-CD8 antibody ($\times 10$), anti-mouse IBA1 antibody ($\times 10$), and anti-mouse CD45 antibody ($\times 10$). a, no treatment; b, unarmed T cells; c, GD2-EATs. **B** Neuroblastoma PDX bearing mice were treated by GD2-EATs with anti-Ly6G antibody to deplete granulocytes. **C** The complete blood count (CBC) test was done and compared among groups. **D** Tumors harvested on day 10 were analyzed by flow cytometry (Additional file 1: Fig. S3), and the frequencies of each tumor infiltrating leukocytes were compared among groups. **E** The PDXs treated with GD2-EATs plus anti-Ly6G antibody were harvested on day 10 after the start of treatment and were stained by anti-human CD3 antibody ($\times 10$), anti-human CD4 antibody ($\times 10$), anti-CD8 antibody ($\times 10$), anti-mouse IBA1 antibody ($\times 10$)

All statistical analyses were performed using GraphPad Prism V.8.0 for Windows (GraphPad Software, La Jolla, CA, www.graphpad.com). P value < 0.05 was considered statistically significant. Asterisks indicate that the experimental P value is statistically significantly different from the associated controls at * $P < 0.05$; ** $P < 0.01$; *** $P < 0.001$, **** $P < 0.0001$.

Results

T-BsAb transformed immunologically ‘cold tumors’ to ‘hot tumors’

We previously demonstrated that ex vivo armed T cells with IgG-[L]-scFv platformed BsAb (EATs) infiltrated solid tumors rapidly and persisted for weeks, leading to complete tumor ablation [25]. Here we administered unarmed T cells or T cells armed with GD2-BsAb (GD2-EATs) into mice xenografted with neuroblastoma PDX (Additional file 1: Fig. S1A). Tumors were analyzed by flow cytometry on day 10 post-treatment (Additional file 1: Fig. S1B). While unarmed T cell-treated or untreated tumors had few leukocytes typical for ‘cold tumors’, those treated with GD2-EATs had plenty of leukocytes, including human T cells and mouse-derived myeloid cells—all characteristics of ‘hot tumors’. In contrast to tumors without treatment or treated with unarmed T cells showing few TIMs, tumors treated with GD2-EATs were infiltrated with higher frequencies of mCD45⁺TIMs, comprising 50% of PMN-MDSCs (CD11b⁺Ly6G⁺Ly6C^{lo}), 20% of TAMs (CD11b⁺Ly6G⁻Ly6C^{lo}F4/80⁺), 11% of M-MDSCs (CD11b⁺Ly6G⁻Ly6C^{hi}), and 17% of Ly6C^{lo} MDSCs (CD11b⁺Ly6G⁻Ly6C^{lo}F4/80⁻), respectively. When tumors were studied by IHC (Fig. 1A), the tumors in control groups (unarmed T cells or no treatment) showed few leukocytes, whereas GD2-EAT-treated tumors had diffuse T cell infiltration along with strong positivity for mouse myeloid cell markers, i.e., mCD45 and IBA1 (ionized calcium-binding adaptor molecule-1) staining. These findings were confirmed in 143B osteosarcoma CDX model (Additional file 1: Fig. S2). The tumors treated with GD2-BsAb plus human PBMCs presented

robust CD11b⁺TIM infiltration with diffuse CD3⁺T cell infiltration, contrasting with the tumors treated with PBMCs alone which had few leukocyte infiltrates.

TIM depletion enhanced anti-tumor effect of T-BsAb Granulocyte depletion

Although T-BsAb successfully transformed ‘cold tumors’ to immunologically ‘hot tumors’, not all tumors responded to treatment. To test if removing TIMs could enhance anti-tumor response of T-BsAb, we selectively depleted each TIM and studied the effect on BsAb-driven T cell trafficking, infiltration, and in vivo anti-tumor response.

In order to deplete PMN-MDSCs, anti-Ly6G antibody was administered one day before each GD2-EAT treatment (Fig. 1B). After 2 doses of anti-Ly6G antibody and GD2-EATs, peripheral blood (PB) was collected for CBC (Fig. 1C). Anti-Ly6G antibody successfully removed neutrophils but did not affect monocytes in the circulation. The neuroblastoma PDXs were harvested on day 10 post-treatment and analyzed by flow cytometry (Fig. 1D and Additional file 1: Fig. S3). When compared to the tumors treated with GD2-EATs alone, anti-Ly6G combination significantly reduced the frequency of mLy6G⁺PMN-MDSCs ($P < 0.0001$) without affecting mCD11b⁺F4/80⁺ TAMs. This was accompanied by a reciprocal increase in human T cells, mLy6C^{hi} M-MDSCs, and mLy6C^{lo} MDSCs ($P = 0.039$, $P = 0.014$, and $P < 0.0001$, respectively). IHC staining of tumors confirmed the inverse relationship of granulocyte depletion and enhanced T cell infiltration, for both CD4⁺ and CD8⁺T cells (Fig. 1E). Macrophage-specific protein IBA1 staining of tumors did not show significant difference compared to tumors treated with GD2-EATs alone. To quantify T cell infiltration in tumors and characterize T cell populations, positive pixel count analysis was performed on IHC slides stained with antibodies against CD3, CD4, and CD8 (Supplementary Table S1) [26]. Tumors treated with GD2-EATs plus anti-Ly6G showed 3.8-fold increase of CD3, 5.8-fold increase of CD4, and 4.8-fold increase of CD8 T cell infiltration compared

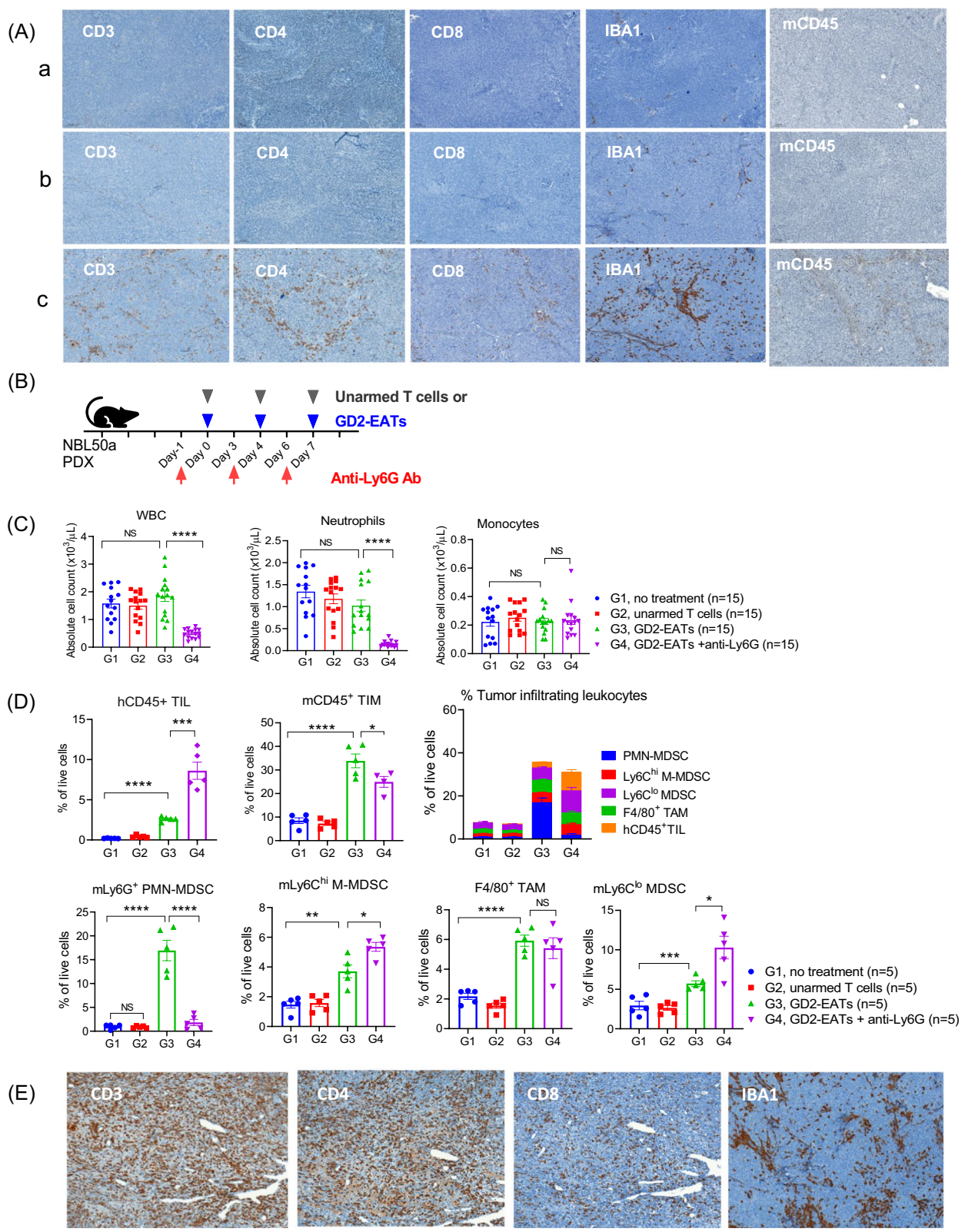


Fig. 1 (See legend on previous page.)

(See figure on next page.)

Fig. 2 The effects of granulocyte depletion on BsAb directed T cell trafficking and in vivo anti-tumor response. **A** Luciferase transduced T cells [Luc(+)-T cells] were administered with GD2-BsAb and anti-GR1 or anti-Ly6G antibody to treat small cell lung cancer cell line (NCI-N417) xenografts. Luc(+)-T cells were administered intravenously (iv) on day 0, and GD2-BsAbs were iv administered on day 0 and day 5 separately. Anti-Ly6G or anti-GR1 antibodies were administered on day -1 and day 4 intraperitoneally. **B** Bioluminescence of Luc(+)-T cells infiltrated into tumors were monitored. The bioluminescence images on day 4 and quantification of the bioluminescence in the lesions of tumor. Control BsAb, Luc(+)-T cells plus control BsAb; GD2-BsAb, Luc(+)-T cells plus GD2-BsAb; GD2-BsAb plus anti-GR1, Luc(+)-T cells plus GD2-BsAb plus anti-GR1 antibody; GD2-BsAb plus anti-Ly6G, Luc(+)-T cells plus GD2-BsAb plus anti-Ly6G antibody. **C** In vivo anti-tumor response by GD2-BsAb and granulocyte depleting antibodies was tested against melanoma cell line (M14) xenografts. Control BsAb, Luc(+)-T cells plus control BsAb; GD2-BsAb, Luc(+)-T cells plus GD2-BsAb; GD2-BsAb+ anti-GR1, Luc(+)-T cells plus GD2-BsAb plus anti-GR1 antibody; GD2-BsAb+ anti-Ly6G, Luc(+)-T cells plus GD2-BsAb plus anti-Ly6G antibody. **D** In vivo anti-tumor effect of GD2-EATs with anti-Ly6G antibody was tested against neuroblastoma patient-derived xenografts (PDXs), and long-term survival was analyzed

to GD2-EATs alone ($P=0.005$, $P=0.02$, and $P=0.003$, respectively).

The effect of granulocyte depleting antibodies was also tested in 143B osteosarcoma cell line xenograft mouse model (Additional file 1: Fig. S4A). Anti-GR1 or anti-Ly6G antibody was administered with GD2-EATs or unarmed T cells. CBC analyses on day 5 showed that anti-Ly6G or anti-GR1 antibody significantly decreased neutrophil count in the circulation, while anti-GR1 depleted monocytes as well (Additional file 1: Fig. S4B). Tumors were harvested and analyzed on day 60 post-treatment (Additional file 1: Fig. S4C). Anti-GR1 or anti-Ly6G antibody significantly increased the frequencies of hCD45⁺ or hCD8⁺ TILs by flow cytometry, confirming the effect by anti-human CD3 IHC staining of tumors (Additional file 1: Fig. S4D).

To study the effect of granulocyte depletion on BsAb-driven T cell trafficking, luciferase labeled T cells [Luc(+)-T cells] and soluble GD2-BsAb were administered to mice xenografted with GD2(+)-small cell lung cancer (SCLC) cell line NCI-N417 one day after iv treatment of anti-Ly6G or anti-GR1 antibody (Fig. 2A). Luciferase signals in the tumors were monitored, and mean bioluminescence intensity (total flux, photon/sec) of TILs was compared among groups (Fig. 2B). In contrast to control BsAb, GD2-BsAb successfully drove Luc(+)-T cells into xenografts, and the addition of anti-GR1 or anti-Ly6G antibody amplified the bioluminescent intensity (BLI) in tumors more than two-fold above those treated with GD2-BsAb. In addition, these granulocyte depleting antibodies delayed the loss of bioluminescence from the tumors. BLI by day 11 has dropped to 1% of its peak in the GD2-BsAb group. In contrast, with the addition of anti-Ly6G or anti-GR1 antibody, the BLI by day 11 was 10 to 50-fold higher compared to GD2-BsAb ($P=0.009$). The enhanced BLI of TILs by depleting granulocytes was confirmed again in neuroblastoma PDX model (Additional file 1: Fig. S5). Area under curves (AUC) of the BLI analyzed to estimate the total quantity of TILs increased by an average of 2.9-fold to 5.5-fold in the anti-Ly6G or

anti-GR1 combination treatment groups, respectively (Supplementary Table S2).

The enhancement of T cell infiltration and persistence in tumors by granulocyte depletion translated to a substantial improvement in anti-tumor effect in vivo. In contrast to control-BsAb where tumors grew unabated, GD2-BsAb treatment suppressed tumor growth, and the anti-tumor response against melanoma cell line (M14) xenografts was much enhanced by granulocytes depletion ($P=0.01$) (Fig. 2C). The in vivo anti-tumor effect was also tested in neuroblastoma PDX (Fig. 2D) and osteosarcoma CDX models (Additional file 1: Fig. S4E). Anti-Ly6G antibody improved in vivo efficacy of GD2-EATs against neuroblastoma PDXs ($P=0.003$) and prolonged survival ($P=0.002$). Osteosarcoma xenografts also demonstrated the benefit of anti-GR1 or anti-Ly6G antibody, with improved tumor control and overall survival compared to GD2-EATs alone ($P=0.024$).

Monocyte depletion

Anti-Ly6C antibody was applied to deplete M-MDSC one day before GD2-EATs injection in a neuroblastoma PDX mouse model (Fig. 3A). After 2 doses of anti-Ly6C antibody and GD2-EATs, PB was collected for CBC analyses (Fig. 3B). Anti-Ly6C antibody successfully depleted monocytes without affecting neutrophils in the circulation. Tumors were harvested on day 10 post-treatment and analyzed by flow cytometry (Fig. 3C and Additional file 1: Fig. S3). After anti-Ly6C antibody treatment, the frequencies of mLy6C^{hi} M-MDSCs and F4/80⁺ TAMs decreased when compared to GD2-EATs alone ($P=0.004$ and $P=0.04$, respectively). While the frequency of mLy6G⁺ PMN-MDSC increased, that of Ly6C^{lo} MDSC did not change. In the presence of anti-Ly6C antibody, GD2-EAT treated tumors showed more robust hCD45⁺ TIL infiltration than tumors treated with GD2-EATs alone. IHC staining using anti-human CD3, CD4, and CD8 antibody confirmed the increase of TILs when treated with GD2-EATs in the presence of anti-Ly6C antibody (Fig. 3D). Tumors treated with

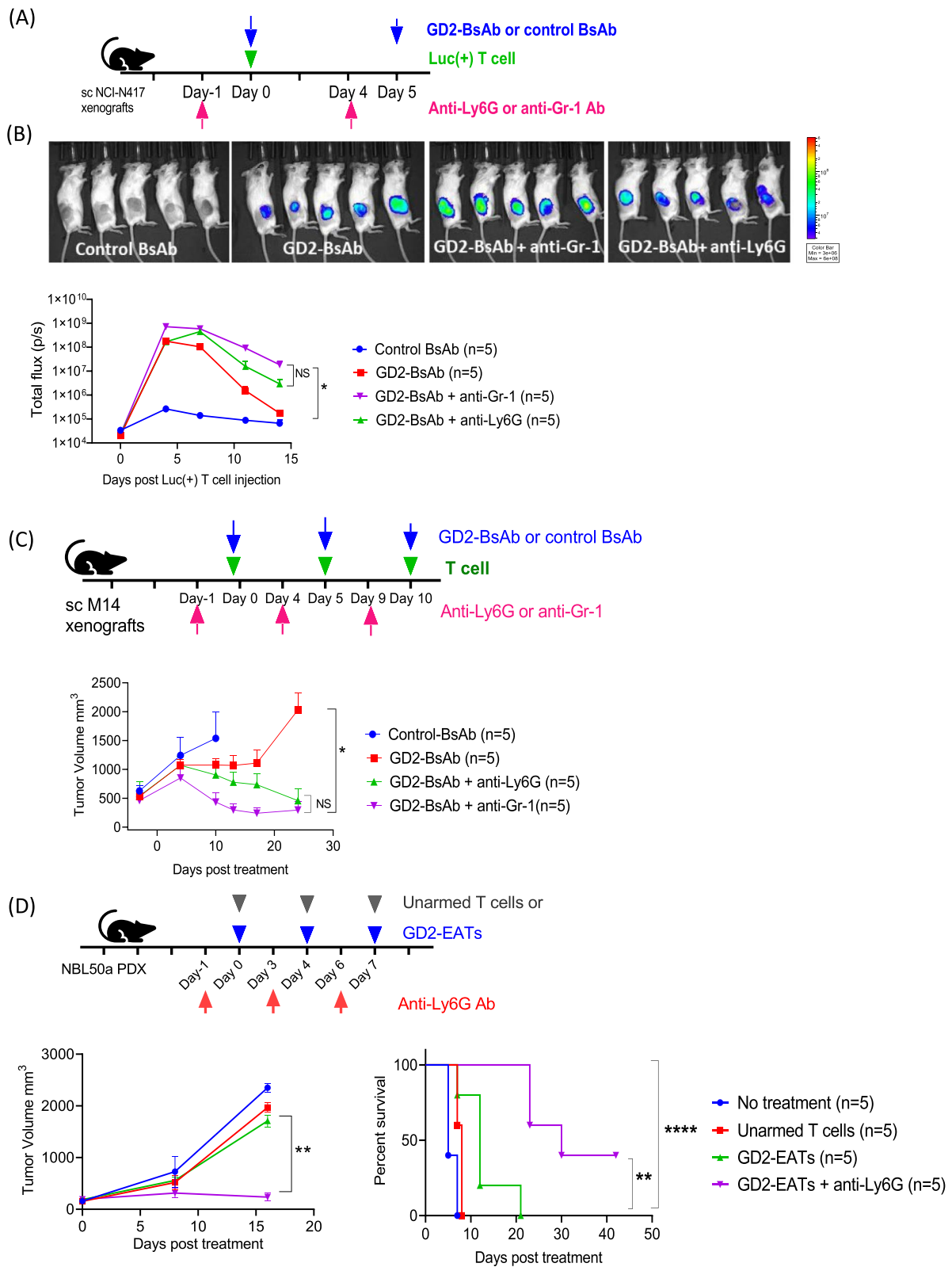


Fig. 2 (See legend on previous page.)

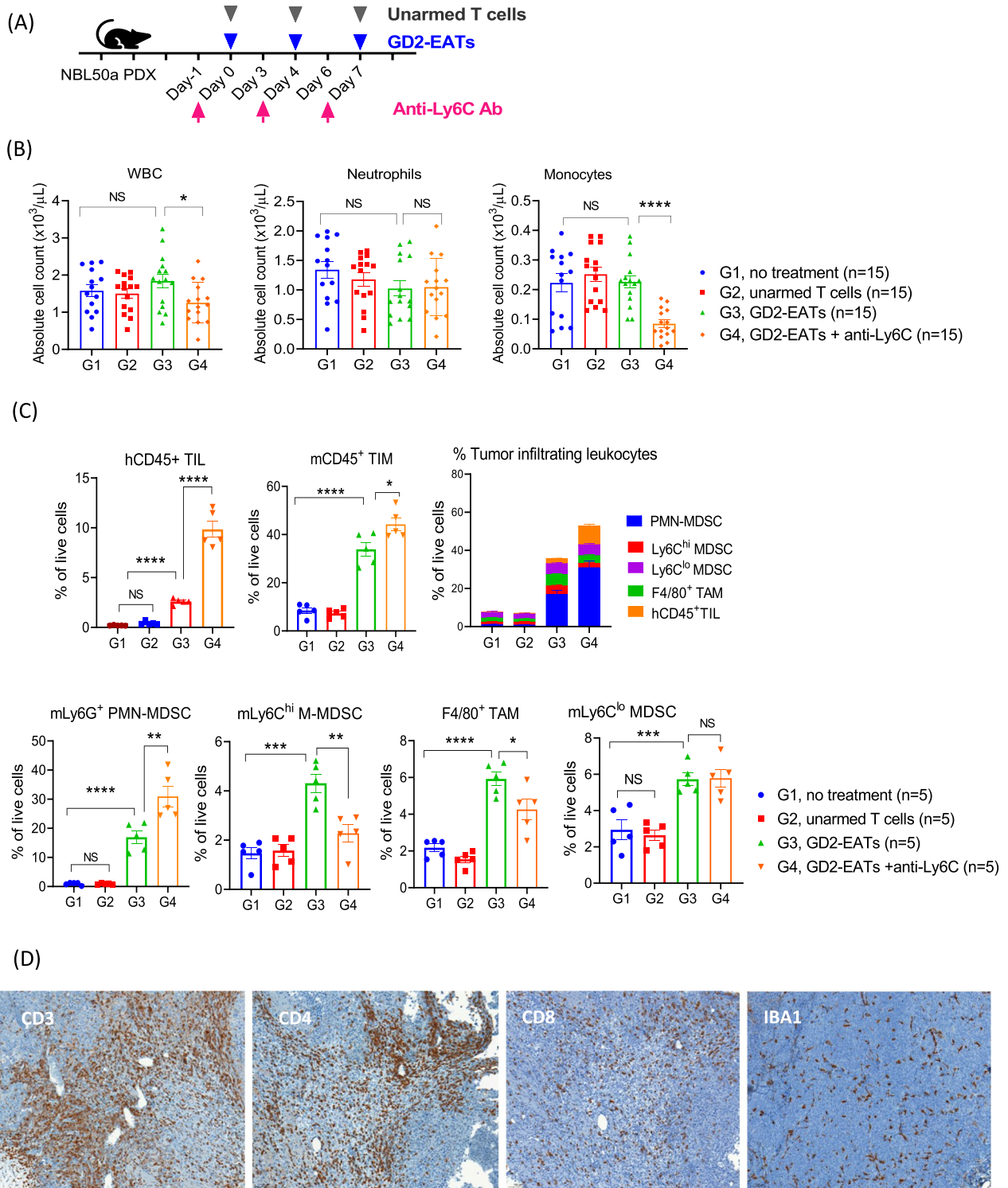


Fig. 3 The effects of monocyte depletion on BsAb directed T cell immunotherapy. **A** Neuroblastoma PDX bearing mice were treated by GD2-BsAb armed T cells (GD2-EATs) with anti-Ly6C antibody to deplete monocytes. **B** Peripheral blood (PB) was analyzed by CBC and compared among groups. **C** Tumors harvested on day 10 were analyzed by flow cytometry (Additional file 1: Fig. S3), and the frequencies of each tumor infiltrating leukocytes were compared among groups. **D** Immunohistochemical (IHC) staining of tumor sections by anti-human CD3 antibody ($\times 10$), anti-human CD4 antibody ($\times 10$), anti-CD8 antibody ($\times 10$), and anti-mouse IBA1 antibody ($\times 10$). The tumors were harvested on day 10 after the start of treatment

(See figure on next page.)

Fig. 4 The effects of monocyte depletion on BsAb directed T cell trafficking and in vivo anti-tumor response. **A** Luciferase transduced T cells [Luc(+)] or Luciferase transduced GD2-BsAb armed T cells [Luc(+)] GD2-EATs were administered with anti-Ly6C antibody to the mice bearing neuroblastoma patient-derived xenograft (PDX). **B** Bioluminescence in the lesions of tumor was monitored. The bioluminescence images on day 7 and quantification of the bioluminescence in the lesions of tumor. **C** In vivo anti-tumor response by GD2-EATs with anti-Ly6C antibody was tested against neuroblastoma PDXs. **D** In vivo anti-tumor effect of GD2-EATs with anti-Ly6C antibody was tested against osteosarcoma PDXs, and long-term survival was analyzed

GD2-EATs plus anti-Ly6C showed 2.3-fold increase of CD3, 3.2-fold increase of CD4, and fourfold increase of CD8 T cell infiltration compared to GD2-EATs alone by positive pixel count analysis ($P=0.023$, $P=0.083$, and $P=0.1522$, respectively) (Supplementary table S1).

These effects of anti-Ly6C antibody were reproduced in the osteosarcoma tumor model (Additional file 1: Fig. S6A). CBC analyses on day 5 showed a significant decrease of monocyte count (Additional file 1: Fig. S6B). Tumors were harvested on day 60 post-treatment and analyzed for T cell infiltration. The frequency of hCD45⁺TIL or hCD8⁺ TIL was significantly higher after treatment of Ly6C and GD2-EATs combination compared to GD2-EATs alone by flow cytometry ($P=0.044$ and $P=0.045$, respectively) (Additional file 1: Fig. S6C). CD3 IHC staining also showed increased intratumoral GD2-EAT infiltration following anti-Ly6C antibody (Additional file 1: Fig. S6D).

To study the effect of M-MDSCs depletion on T cell trafficking, anti-Ly6C antibody was administered with Luc(+) GD2-EATs in neuroblastoma PDX model (Fig. 4A). Unlike the Luc(+) unarmed T cells which disappeared following a transit sequestration in the lungs, the Luc(+) GD2-EATs efficiently trafficked to the tumor sites and persisted longer, as evidenced by their bioluminescence (Fig. 4B). Anti-Ly6C antibody significantly enhanced peak BLI in the tumors ($P=0.02$) while delaying their disappearance, with bioluminescence remained 20-fold higher when compared to GD2-EATs alone on day 12 ($P=0.006$). Total quantity of TILs assessed by AUC of the BLI increased by 3.5-fold compared to GD2-EATs alone (Supplementary Table S2).

Depletion of M-MDSCs was associated with significantly improved tumor control as well. Neuroblastoma PDXs treated by GD2-EATs combined with anti-Ly6C antibody showed improved tumor control compared to GD2-EATs alone ($P=0.04$) and enhanced survival ($P=0.008$) (Fig. 4C). In a separate set of experiments using osteosarcoma PDXs, while 3 of 4 mice treated with GD2-EATs experiencing tumor relapse, all 4 mice treated with GD2-EATs plus anti-Ly6C antibody showed a long-term remission (> 180 days post treatment), demonstrating the benefit of depleting M-MDSCs ($P=0.04$), (Fig. 4D). The benefit of anti-Ly6C antibody was verified again in osteosarcoma cell line derived xenografts

(CDXs) (Additional file 1: Fig. S6), where anti-Ly6C antibody increased intratumoral infiltration of GD2-EATs when compared with GD2-EATs alone, thereby translating to enhanced in vivo anti-tumor response ($P=0.006$).

Macrophage depletion

We treated mice with either clodronate liposome (CL) or anti-CSF1R antibody to deplete macrophages and investigated their effect on T-BsAb treatment. After 2 doses of each treatment, macrophages were depleted from the liver or the spleen (Additional file 1: Fig. S7A and Fig. S7B). Neuroblastoma PDXs were treated with GD2-EATs and anti-CSF1R antibody or CL (Fig. 5A). CBC analyses after 2 doses of anti-CSF1R antibody or CL did not show significant differences among treatment groups: anti-CSF1R antibody or CL did not affect neutrophils or monocytes in the circulation (Fig. 5B). When tumors were analyzed on day 10 (Fig. 5C and Additional file 1: Fig. S3), anti-CSF1R antibody and CL significantly increased hCD45⁺ TILs and mCD45⁺ TIMs by flow cytometry. While the tumors showed a marked reduction of CD11b⁺F4/80⁺ TAMs and Ly6C^{hi} M-MDSCs, there was an increase in Ly6G⁺ PMN-MDSCs and Ly6C^{lo} MDSCs. IHC staining of tumors on day 10 showed that macrophage depletion greatly promoted BsAb-driven T cell infiltration reversely to the decrease of IBA-1(+) macrophages (Fig. 5D). The tumors treated with GD2-EATs plus anti-CSF1R showed 4.7-fold increase of CD3, 5.3-fold increase of CD4, and 17.8-fold increase of CD8 T cell infiltration compared to GD2-EATs alone ($P=0.009$, $P=0.028$, and $P=0.026$, respectively); the tumors treated with GD2-EATs plus CL presented a 4.4-fold increase of CD3, 5.8-fold increase of CD4, and 15-fold increase of CD8 T cell infiltration by positive pixel count analyses ($P<0.0001$, $P=0.009$, and $P=0.0074$, respectively), (Supplementary Table S1). In addition, the tumors treated with GD2-EATs plus anti-CSF1R antibody or CL showed a significant increase in CD8 to CD4 TIL ratios compared to GD2-EATs alone ($P=0.001$ and $P=0.0001$, respectively). The enhancement of T cell infiltration by anti-CSF1R antibody or CL was also observed in 143B osteosarcoma CDXs (Additional file 1: Fig. S7C) and M14 melanoma CDXs (Additional file 1: Fig. S7D).

We next studied the effect of macrophage depletion on BsAb-driven T cell trafficking into solid tumors. Luc(+)

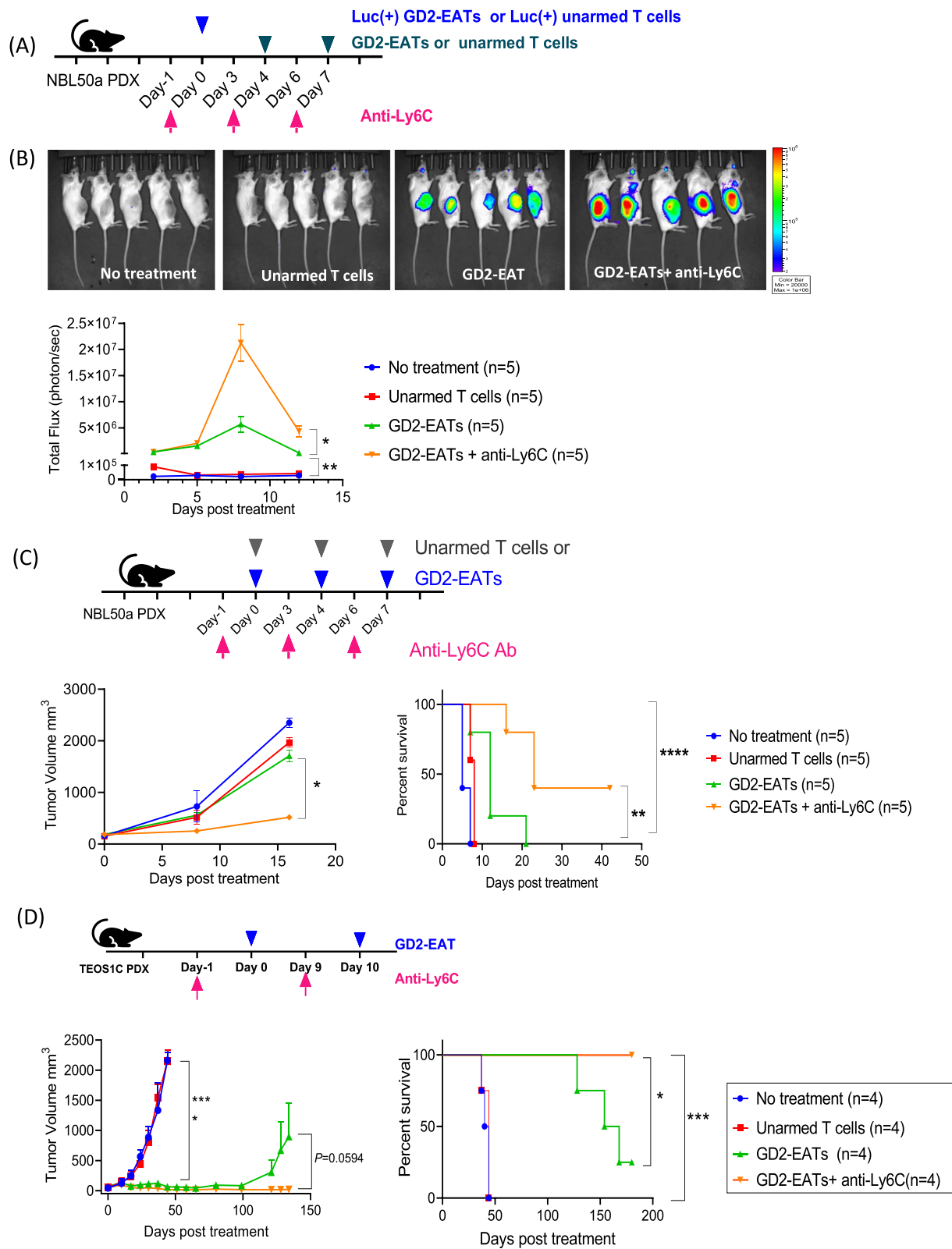


Fig. 4 (See legend on previous page.)

(See figure on next page.)

Fig. 5 The effects of macrophage depletion on BsAb directed T cell immunotherapy. **A** Neuroblastoma PDX bearing mice were treated by GD2-BsAb armed T cells (GD2-EATs) with anti-CSF1R antibody or clodronate liposome (CL) to deplete macrophages. **B** Peripheral blood (PB) was analyzed by CBC and compared among groups. **C** Tumors harvested on day 10 were analyzed by flow cytometry (Additional file 1: Fig. S3), and the frequencies of each tumor infiltrating leukocytes were compared among groups. **D** Immunohistochemical (IHC) staining of tumor sections by anti-human CD3 antibody (× 10), anti-human CD4 antibody (× 10), anti-CD8 antibody (× 10), and anti-mouse IBA1 antibody (× 10). The tumors were harvested on day 10 after the start of treatment

GD2-EATs was administered with anti-CSF1R antibody or CL to neuroblastoma PDX bearing mice (Fig. 6A), and the BLI in tumors were quantified (Fig. 6B). Anti-CSF1R antibody or CL significantly increased the BLI in tumors treated with GD2-EATs (3.2-fold and 6.6-fold increase, respectively, Supplementary Table S2). The effect of CL on BsAb-driven T cell trafficking was also tested in SCLC CDXs (Additional file 1: Fig. S8A). With CL, the bioluminescence of T cell persisted through day 11, being 100-fold higher than those for GD2-BsAb alone ($P=0.02$). The effect of anti-CSF1R antibody was also verified in an osteosarcoma PDX model (Additional file 1: Fig. S8B), where the mean BLI in tumors treated with HER2-EATs plus anti-CSF1R antibody was 40-fold higher than those for HER2-EATs alone on day 11 ($P=0.022$). Based on the AUC of the BLI, the total quantity of TILs in tumors increased 4.5-fold and 3.6-fold in the presence of CL and anti-CSF1R antibody, respectively (Supplementary Table S2).

The enhanced T cell infiltration by macrophage depletion translated to improved anti-tumor response. Anti-CSF1R antibody or CL significantly enhanced tumor suppressive effect of GD2-EATs and prolonged survival without significant toxicity, surpassing the efficacy of G-MDSCs or M-MDSC depleting treatment (Fig. 6C). M14 xenografts treated with soluble GD2-BsAb plus CL showed complete regression despite large tumor volume at the beginning of treatment, contrasting to GD2-BsAb alone (without CL) where tumor grew unabated (Fig. 6D). The enhanced anti-tumor effect of macrophage depletion was confirmed in osteosarcoma PDX and 143B CDX models (Additional file 1: Fig. S9). CL or anti-CSF1R antibody significantly improved anti-tumor response of GD2-EATs without increasing toxicity, prolonging survival.

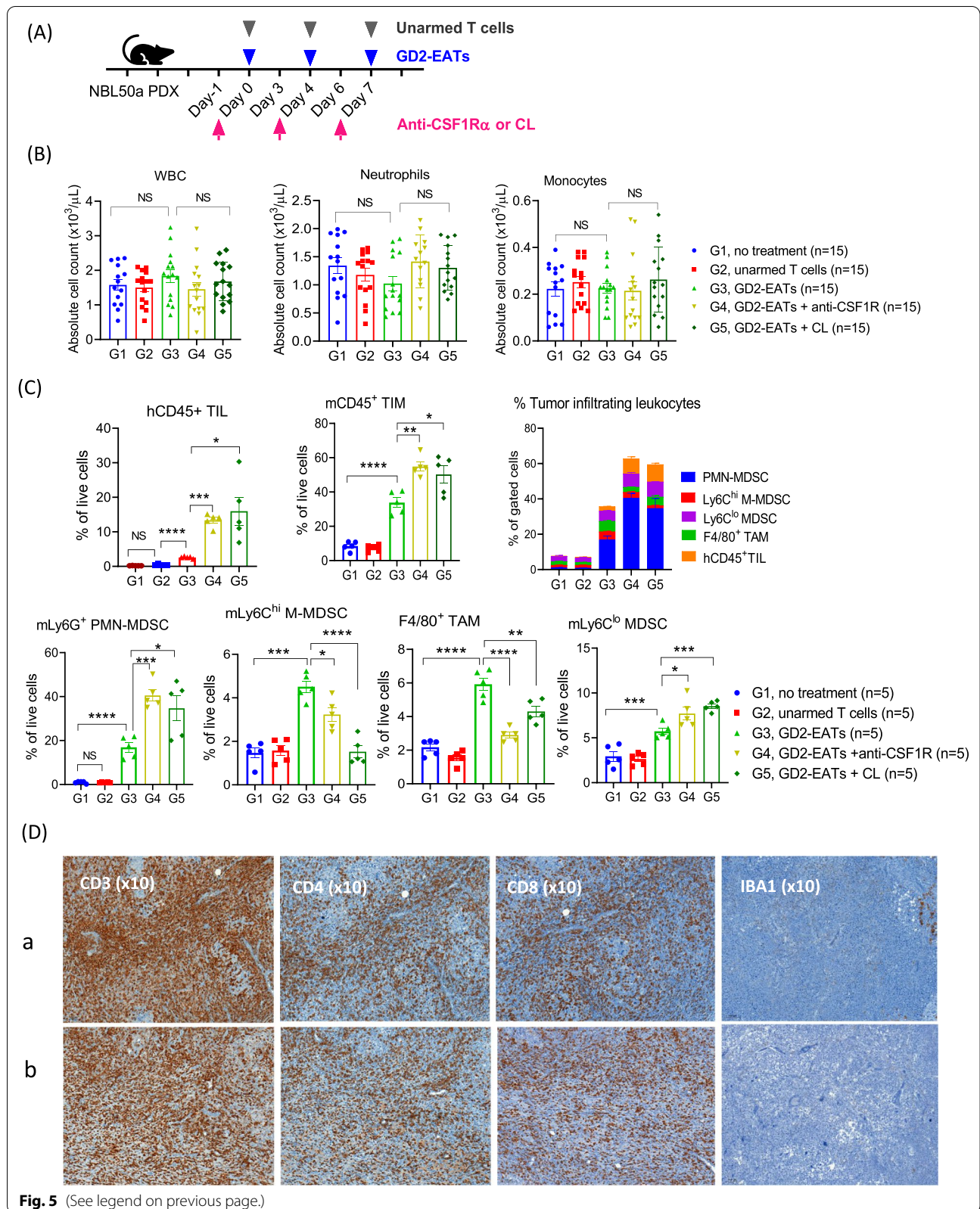
Corticosteroid premedication to modulate TIMs

Corticosteroid was tested for their anti-inflammatory effect on TIM and TIL, since it is often used as a premedication to mitigate cytokine release during BsAb treatment. We tested increasing dose levels of dexamethasone [low-dose (LD); 2 mg/kg/dose, intermediate-dose (ID); 8 mg/kg/dose, and high-dose (HD); 32 mg/kg/dose], equivalent to 0.16 mg/kg to 2.6 mg/kg of human dose [27], as a premedication before each GD2-EAT treatment

(Fig. 7A). Cytokine levels were analyzed at different time points post-treatment (Additional file 1: Fig. S10). Dexamethasone premedication decreased IL-2, IL-6, and TNF- α release from GD2-EATs, while IFN- γ levels were not significantly affected. After 2nd treatment dose, PB leukocytes were analyzed by CBC (Fig. 7B). Dexamethasone profoundly reduced monocytes but did not significantly affect neutrophils in the circulation. Dexamethasone also affected the frequencies of tumor infiltrating leukocytes by flow cytometry analyses (Fig. 7C and Additional file 1: Fig. S11). The increase in mCD45⁺ TIM and mLy6G⁺ PMN-MDSC was dexamethasone dose-dependent ($P=0.0001$ and $P=0.0003$, respectively). Ly6C^{hi} M-MDSCs were depleted by HD dexamethasone ($P=0.006$), accompanied by an increase in the proportion of Ly6C^{lo} MDSC. Most notable was the decrease in the frequencies of mCD11b⁺F4/80⁺ TAMs following dexamethasone treatment ($P=0.0001$). The depletion of TAMs was dose-dependent, being most apparent with HD dexamethasone (no dexamethasone vs. LD, $P=0.35$; vs. ID, $P=0.002$; vs. HD, $P<0.0001$). Dexamethasone increased the frequency of hCD45⁺ TIL ($P=0.0007$), and in particular CD8⁺ TIL in a dose-dependent fashion ($P=0.015$), demonstrating an inverse correlation with TAMs. This effect of dexamethasone on intratumoral T cell infiltration was confirmed by IHC staining using anti-human CD3 antibody (Fig. 7D). Tumors treated with GD2-EAT plus ID or HD dexamethasone showed more abundant TILs compared to GD2-EATs alone ($P<0.0001$).

The effect of dexamethasone premedication on BsAb-driven T cell trafficking was studied using an osteosarcoma PDX model (Additional file 1: Fig. S12). Intratumoral bioluminescence of Luc(+) GD2-EAT or Luc(+) unarmed T cell was quantified and compared among groups treated with increasing doses of dexamethasone. The BLI of tumors treated with GD2-EATs plus ID dexamethasone was tenfold higher than those for GD2-EATs alone on day 5, and the bioluminescence persisted throughout day 14. When estimated by BLI AUC, the total quantity of TILs increased 7.7-fold and 14-fold by LD- and ID-dexamethasone, respectively (Supplementary Table S2).

In vivo anti-tumor response also correlated with the BLIs in tumors and the frequencies of TIL.



(See figure on next page.)

Fig. 6 The effects of macrophage depletion on BsAb directed T cell trafficking and in vivo anti-tumor response. **A** Luciferase transduced T cells [Luc(+)-T cells] or Luciferase transduced GD2-BsAb armed T cells [Luc(+)-GD2-EATs] were administered with anti-CSF1R antibody or clodronate liposome (CL) to the mice bearing neuroblastoma patient-derived xenograft (PDX). **B** Bioluminescence in the lesions of tumor was monitored. The bioluminescence images on day 7 and quantification of the bioluminescence in the lesions of tumor. **C** In vivo anti-tumor response by GD2-EATs with anti-CSF1R antibody or CL was tested against neuroblastoma PDXs. **D** GD2-BsAb and T cells were separately administered intravenously with or without intraperitoneal CL. In vivo anti-tumor effect of GD2-BsAb with CL was tested against M14 melanoma cell line xenografts and compared with control BsAb or GD2-BsAb without CL

Dexamethasone did not compromise anti-tumor effect of GD2-BsAb against neuroblastoma PDXs (Fig. 7E and Additional file 1: Fig. S13A). Irrespective if administered as direct BsAb injection or as EATs, ID and HD dexamethasone enhanced the anti-tumor effect of GD2-BsAb, with significant improvement in survival ($P < 0.0001$). This favorable effect of dexamethasone on GD2-EATs was confirmed in another osteosarcoma PDX model. When LD (2 mg/kg) or ID (8 mg/kg) dexamethasone was premedicated, tumor control and survival improved in a dose-dependent manner with statistical significance (Additional file 1: Fig. S13B).

Discussion

T-BsAbs built on the IgG-[L]-scFv platform, whether administered as stand-alone or as EATs are effective in driving T cells into solid tumors and inducing cytotoxic anti-tumor response against a number of cancer targets [22, 28–30]. Together with myeloid cells, these BsAb-driven T cells transformed immunologically ‘cold tumors’ into ‘hot tumors.’ Using antibodies specific to deplete TIM subsets, we analyzed the PMN-MDSC, M-MDSC, and TAM following T-BsAb treatment. Based on selective myeloid cell depleting antibodies, we tested their role in human T cell infiltration into human tumors and in vivo anti-tumor response of BsAb treatment. Each of the myeloid cell inhibitors, including anti-Ly6G, anti-GR1, anti-Ly6C, anti-CSF1R antibodies, and CL decreased their respective mouse TIM subsets, enhancing T-BsAb-driven T cell infiltration and persistence, resulting in improved anti-tumor response. Dexamethasone premedication reduced circulating monocytes and TAMs in tumors in a dose-dependent manner, followed by a substantial improvement in intratumoral T cell infiltration and anti-tumor efficacy of BsAb treatment.

When we compared anti-tumor benefit from depletion of each myeloid cell, the most effective was macrophage depleting strategies. Anti-CSF1R antibody or CL significantly reduced the frequencies of not only mCD11b⁺F4/80⁺ TAM but also mLy6C^{hi} M-MDSC compared to the treatment of GD2-EATs alone, while markedly increasing the frequencies of intratumoral hCD45⁺T cells. IHC staining of neuroblastoma PDXs showed that macrophage depletion significantly

increased not only CD3 T cell infiltration but also CD8 to CD4 TIL ratios compared to GD2-EATs, while anti-Ly6G or anti-Ly6C antibody did not affect this ratio. TAM is one of the formidable obstacles to T cell immunotherapy, especially for solid tumors. While M1 macrophages play a role in human immunity by producing proinflammatory cytokines with strong phagocytic function, TAMs, recruited in TME, not only lack the function of phagocytizing tumor cells but also help tumor cells escape from immune surveillance and metastasize by stimulating angiogenesis and protecting tumor cells from cytotoxic T cells or NK cells [31–33]. In addition, TAMs are reprogrammed towards an iron-releasing phenotype, characterized by higher expression of the iron exporter ferroportin and iron transporter lipocalin-2, which promote tumor progression [34]. CD8⁺ cytotoxic T cells induce ferroptosis in tumor cells [35], and T cell-based immunotherapies including chimeric antigen receptor (CAR) or T-BsAb are likely to act through ferroptosis [36]. Ferroptotic cancer cells release oncogenic KRAS protein which drives macrophages to enrich and switch to an M2-like pro-tumoral phenotype via STAT-dependent fatty acid oxidation [37, 38]. These TAMs exert higher resistance to ferroptosis compared with cancer cells. Moreover, erastin or SLC7A11 depletion to enhance ferroptosis were insufficient to induce macrophage ferroptosis [39, 40], implicating the considerable role of TAMs against T cell induced-anti-tumor response and the substantial benefit of depleting TAMs for T cell immunotherapy.

Depleting myeloid cell populations simultaneously could enhance anti-tumor efficacy of T cell immunotherapy even further, although complete depletion of myeloid cells could substantially increase clinical toxicities. Anti-GR1 antibody depletes both Ly6G⁺ granulocytes and Ly6C^{hi} monocytes simultaneously, while anti-CSF1R antibody depletes resident subset of monocytes and tissue- and tumor-associated macrophages together [41]. When tested their effect, anti-GR1 antibody depleted both granulocytes and monocytes, while anti-Ly6G antibody depleted just granulocytes. Though, anti-GR1 plus GD2-EATs did not produce a significant difference in TILs and in vivo anti-tumor response when compared with anti-Ly6G plus GD2-EATs. We also compared the

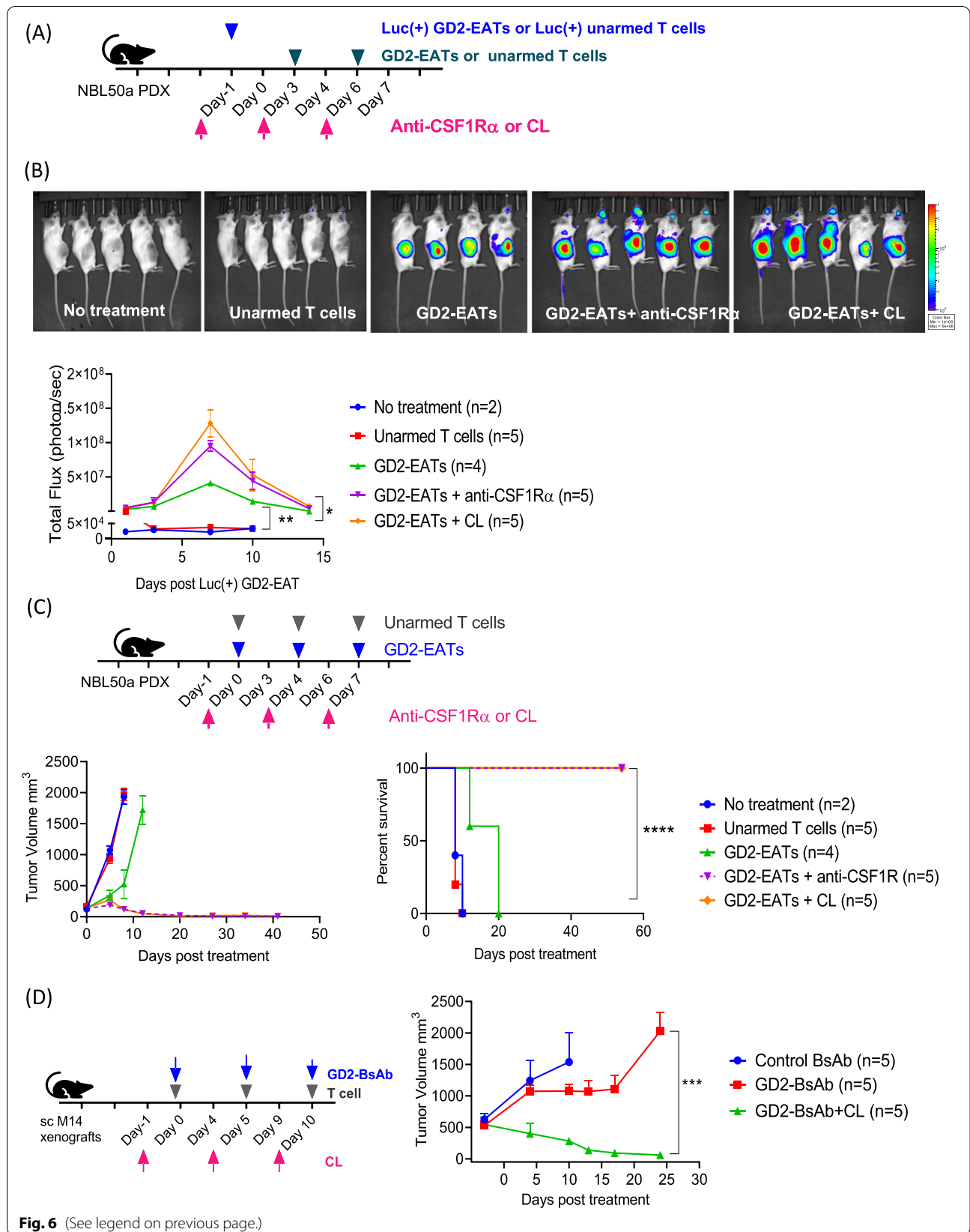


Fig. 6 (See legend on previous page.)

(See figure on next page.)

Fig. 7 The effects of corticosteroids on BsAb directed T cell immunotherapy. **A** Neuroblastoma PDX bearing mice were treated by GD2-BsAb armed T cells (GD2-EATs) with increasing doses of dexamethasone. Dexamethasone was given 1 h before each GD2-EATs or unarmed T cells injection **B** Peripheral blood (PB) was analyzed by CBC and compared among groups. **C** Tumors harvested on day 25 were analyzed by flow cytometry (Additional file 1: Fig. S11), and the frequencies of each tumor infiltrating leukocytes were compared among groups. **D** Immunohistochemical (IHC) staining of tumor sections by anti-human CD3 antibody ($\times 20$) on day 25 after the start of treatment. CD3⁺ T cell numbers were compared by Q-path analysis. G1, no treatment; G2, unarmed T cells; G3, unarmed T cells plus high-dose (HD) dexamethasone; G4, GD2-EATs; G5, GD2-EATs plus low-dose (LD) dexamethasone; G6, GD2-EATs plus intermediate-dose (ID) dexamethasone; G7, GD2-EATs plus high-dose (HD) dexamethasone. **E** In vivo anti-tumor response by GD2-EATs with increasing doses of dexamethasone was tested against neuroblastoma PDXs, and long-term survival was compared among groups

efficacy of anti-CSF1R antibody with anti-Ly6C antibody or CL in neuroblastoma PDX model. Although anti-CSF1R antibody was more effective than anti-Ly6C antibody, it was not superior to CL. The effects of dual depletion of granulocyte and macrophage, or triple depletion of granulocyte, monocytes, and macrophages were not tested in this study, but deserve more in depth investigation.

One of the unexpected findings in our study is the effect of dexamethasone on TIM. Rather than reducing the potency, dexamethasone improved anti-tumor effects of BsAb treatment. The role of dexamethasone on TME and TAMs has not been fully investigated in the new era of T cell immunotherapies. Baseline use of corticosteroids was associated with poor outcome in patients with non-SCLC treated with PD-1 or PD-L1 blockades [42]. But interestingly, while the patients with poor-prognosis appeared to have worse outcome with the use of corticosteroids, those without a history of smoking or poor prognostic factors appeared to have better outcome [42, 43]. Dexamethasone premedication for CD19-BiTE (Blinicyto[®]) did not impair its efficacy [44, 45]. Our study found that dexamethasone premedication did not induce apoptosis of CD8 T cells nor suppress the anti-tumor response of BsAb-driven T cell immunotherapy. On the contrary, it consistently and significantly improved in vivo anti-tumor efficacy of BsAb-driven T cell immunotherapy. Low-dose supplementary IL-2 inhibits dexamethasone-induced apoptosis in CD8 T cells by activating STAT-5 and altering cellular apoptotic potential [46, 47], and TAM suppression by dexamethasone [48] improved the antitumor immune response in cancer xenograft mouse models. Here we showed that dexamethasone depleted monocytes in the circulation and inhibited their recruitment into tumors, thereby decreasing TAMs and Ly6C^{hi} MDSCs, allowing cytotoxic T cells to successfully infiltrate and persist in solid tumors, resulting in significant improvements in anti-tumor response against neuroblastoma and osteosarcoma PDXs. Furthermore, dexamethasone regulates the expression of a huge number of genes in macrophages that are essential for their phagocytic activity, such as glucocorticoid-induced leucine zipper

(Gilz) [49] and Annexin a1 [50–52]. More than 10,000 genomic glucocorticoid receptor (GR) binding sites are induced by dexamethasone in resting macrophages with more than 5,400 known GR target genes [53, 54]. Elucidating the effect of dexamethasone on transcriptomes of TAMs or TILs should yield a deeper insight into the role of glucocorticoid-mediated gene regulation on macrophage and T cell functions, and the mechanisms involved in enhanced anti-tumor efficacy of BsAb-T cell immunotherapies.

Previous studies have shown that tumor infiltrating myeloid cells (TIMs) including MDSCs and TAMs inhibit T cell infiltration into tumors and incapacitate TILs by accelerating T cell exhaustion and dysfunction [1]. The TIMs produce immunosuppressive factors or cytokines, induce Tregs, and drives CD8 T cell exhaustion by upregulation of PD-L1 [4, 55–57]. In this study, depleting TIMs increased TILs: macrophage depletion by anti-CSF1R antibody or CL significantly increased cytotoxic CD8 T cell infiltration. Previously, we showed that the PD-1 expression on CD3 T cells surged around day 16 after GD2-BsAb treatment was started [21], while the neuroblastoma PDXs harvested on day 10 post-treatment had few FoxP3⁺ Tregs irrespective of treatment (Additional file 1: Fig. S14A). When TILs were analyzed on day 60 post-treatment, myeloid cell depleting antibodies significantly increased frequencies of hCD8⁺ TILs, but the PD-1 expression on CD8⁺ TILs was not significantly different among groups ($P=0.45$, Additional file 1: Fig. S14B). In this study, the expression of exhaustion markers with or without depleting antibodies was not investigated in detail. A full kinetic analysis of the exhaustion state of T cells following TIM depletion using extensive flow cytometry profiles and T cell RNA sequencing analysis should provide more insight and will be a subject of a future manuscript.

Despite these TIM depleting treatments, flow cytometry analysis of tumors exhibited a consistent presence of Ly6C^{lo} MDSCs in tumors. Ly6C^{lo} monocytes or Ly6C^{lo} MDSCs are known to express high levels of immunosuppressive proteins and soluble mediators, such as indoleamine 2,3-dioxygenase (IDO)

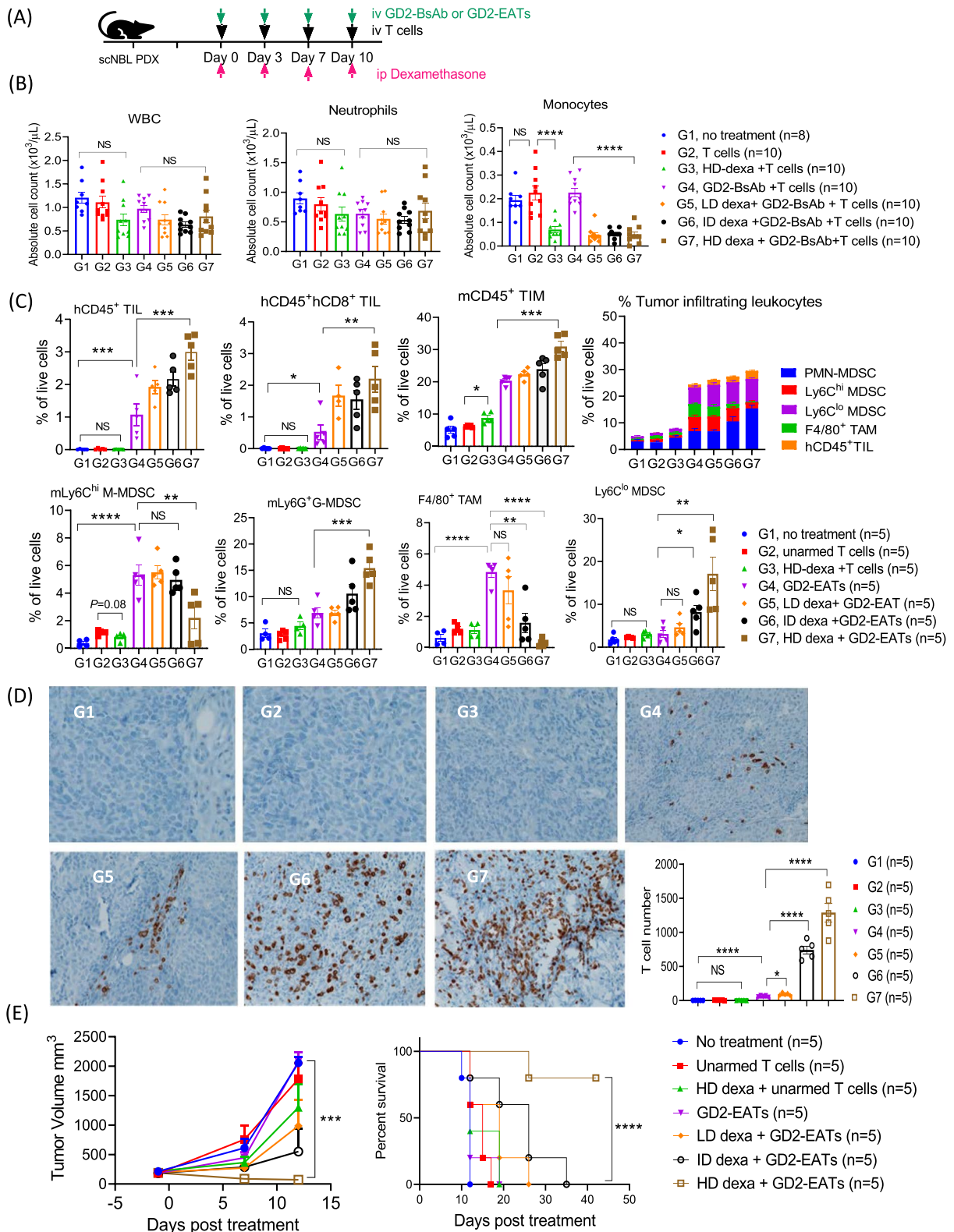


Fig. 7 (See legend on previous page.)

and arginase, interfering CD8⁺T cell proliferation and IFN- γ production [58, 59]. Although anti-Ly6C antibody did not induce a significant change, anti-Ly6G antibody, anti-CSF1R antibody, CL, and dexamethasone all increased Ly6C^{lo} MDSCs in tumors inversely to each depleted myeloid cell population. Macrophages and MDSCs are likely derived from CD11b⁺Ly6G⁻Ly6C^{lo} common myeloid progenitor (CMP) or granulocyte monocyte progenitor (GMP)-like precursors [60, 61], where M-MDSCs differentiate into PMN-MDSCs within the TME through the activity of IRF8 [61–64]. TIM depleting strategies could increase CD11b⁺Ly6G⁻Ly6C^{lo} precursor cell production, hence increasing Ly6C^{lo} MDSC. The biochemical and cellular effects of myeloid cell depleting strategies on MDSC and TAM differentiation are likely to be more complex and need to be investigated in depth. In addition, the effect of Ly6C^{lo} monocyte/MDSC targeting treatment such as liposomal doxorubicin [59] on T-BsAb based immunotherapy also needs to be tested.

Limitations of our preclinical model should also be noted. In our experiments, human cancer cell line or patient-derived tumors were passaged in immunodeficient BRG mice. The BsAbs were built for clinical application, specific for human antigens. We used human T cells as effector cells to study their infiltration into human tumor xenografts, whereas TIMs were mouse-derived. Previous studies of human and mouse TIMs have demonstrated how their subpopulation structures were conserved across patients and species, with a near-complete congruence between human and mouse for dendritic cells, monocytes and neutrophils, though not macrophages [65]. We are aware that tumors consist of many non-cancer cells including innate and adaptive immune cells, fibroblasts, endothelial cells, and lymphatics, which all interact to influence tumorigenesis [66, 67]. Given the species specificity of cell to cell, and cytokine or chemokine to receptor interactions, this preclinical model cannot fully represent the interactions between human tumor cells and human TME. Even after we ruled out the allogeneic effect between human T cells and xenografts from different donors [25], there are still the xenogeneic effect of human cells in a murine microenvironment. Although a fully syngeneic mouse model in an immunocompetent host can be used, there are substantial limitations: (1) we cannot study human T cells, (2) the tumors would no longer be human-derived, and (3) the therapeutics need to be reformatted to target mouse tumor cells, and they are highly immunogenic in immunocompetent mice with neutralizing antibodies developed within 2 weeks. In addition, (4) reformulating the therapeutics for a syngeneic immunocompetent mouse system (anti-tumor IgG

and anti-mouse CD3) puts another major limitation on interpreting the results for their clinical application for humans, losing their clinical relevance.

Conclusion

In conclusion, we demonstrated the importance of TIMs in suppressing BsAb-mediated intratumoral T cell infiltration and in vivo anti-tumor activity. We presented the individual contribution of PMN-MDSCs, M-MDSCs, and TAMs using specific myeloid cell depleting antibodies and inhibitors. BsAbs built on the IgG[L]-scFv platform can turn “cold” tumors into “hot” tumors by driving T cells into them. Myeloid cells following the TILs can interfere with T cell functions. Depletion of TIMs using specific antibodies or dexamethasone markedly enhanced the anti-tumor effects of BsAb-driven T cell immunotherapy by increasing intratumoral T cell infiltration and their persistence. TIM depleting strategies could improve the efficacy of BsAb-based T cell immunotherapy. These data support further investigation of the TME to identify the precise phenotypic and molecular profiles of TIMs to expand curative potential of T-BsAb based immunotherapies against solid tumors.

Bispecific antibodies built on the IgG[L]-scFv platform can turn “cold” tumors into “hot” tumors by driving T cells into them. Myeloid cells following the TILs can interfere with T cell functions. Depletion of TIMs using specific antibodies or dexamethasone markedly enhanced the anti-tumor effects of BsAb-driven T cell immunotherapy by increasing intratumoral T cell infiltration and their persistence. TIM depleting strategies could improve the efficacy of BsAb-based T cell immunotherapy.

Abbreviations

AUC: Area under curve; BLI: Bioluminescence intensity; BRG: BALB-Rag2/-IL-2R- γ -KO; BsAb: Bispecific antibody; CAR: Chimeric antigen receptor; CDX: Cell line derived xenograft; CL: Clodronate liposome; CMP: Common myeloid progenitor; EAT: Ex vivo BsAb armed T cells; FBS: Fetal bovine serum; GMP: Granulocyte monocyte progenitor; IACUC: Institutional Animal Care and Use Committee; IDO: Indoleamine 2,3-dioxygenase; IF: Immunofluorescence; IHC: Immunohistochemistry; MDSC: Myeloid-derived suppressor cell; M-MDSC: Monocytic myeloid-derived suppressor cell; NO: Nitric oxide; PB: Peripheral blood; PBMC: Peripheral blood mononuclear cells; PDX: Patient-derived xenograft; PMN-MDSC: Polymorphonuclear myeloid-derived suppressor cell; SCLC: Small cell lung cancer; TAM: Tumor associated macrophage; TIL: Tumor infiltrating lymphocyte; TIM: Tumor infiltrating myeloid cells; TME: Tumor microenvironment.

Supplementary Information

The online version contains supplementary material available at <https://doi.org/10.1186/s13045-021-01156-5>.

Additional file 1. Supplementary Table S1. Distribution of CD3, CD4, and CD8 T cells in neuroblastoma patient-derived xenografts by positive pixel count analyses. Abbreviations; CL, clodronate liposome.

Supplementary Table S2. Tumor-infiltrating lymphocytes quantified by the area under each BLI curves. Supplementary Table S2. Tumor-infiltrating lymphocytes are quantified by the area under each BLI curve. Abbreviations; SCLC, small cell lung carcinoma; CDX, cell line-derived xenograft; PDX, patient-derived xenograft; CL, clodronate liposome; LD, low-dose; ID, intermediate-dose. **Supplementary Fig. S1.** (A) Neuroblastoma PDX bearing mice were treated by GD2-BsAb armed T cells (GD2-EATs) or unarmed T cells. (B) Tumors were harvested on day 10 and analyzed by flow cytometry. G-MDSC was gated as anti-mouse CD45+CD11b+Ly6G+; M-MDSC was gated as anti-mouse CD45+CD11b+Ly6G-Ly6Chi; TAM was gated as anti-mouse CD45+CD11b+Ly6G-Ly6CloF4/80+; Ly6Clo MDSC was gated as anti-mouse CD45+CD11b+Ly6G-Ly6CloF4/80-. The frequencies of each tumor-infiltrating leukocyte were compared among groups: a, no treatment; b, unarmed T cells; c, GD2-EATs. **Supplementary Fig. S2.** (A) Peripheral blood mononuclear cells (PBMCs) and GD2-BsAb were administered intravenously to the mice bearing 143B osteosarcoma cell line-derived xenograft (CDX). (B) Tumors were harvested on day 14 and immunohistochemical (IHC) stained with anti-CD11b antibody and anti-CD3 antibody. **Supplementary Fig. S3.** (A) Tumors were harvested on day 10 and analyzed by flow cytometry. G-MDSC was gated as anti-mouse CD45+CD11b+Ly6G+; M-MDSC was gated as anti-mouse CD45+CD11b+Ly6G-Ly6Chi; TAM was gated as anti-mouse CD45+CD11b+Ly6G-Ly6CloF4/80+; Ly6Clo MDSC was gated as anti-mouse CD45+CD11b+Ly6G-Ly6CloF4/80-. a, GD2-EATs; b, GD2-EATs plus anti-Ly6G antibody; c, GD2-EATs plus anti-Ly6C antibody; d, GD2-EATs plus anti-CSF1R antibody; e, GD2-EATs plus clodronate liposome (CL). **Supplementary Fig. S4.** (A) Osteosarcoma cell line xenografts were treated by GD2-BsAb armed T cells (GD2-EATs) or unarmed T cells with anti-Gr1 antibody or anti-Ly6G antibody. (B) CBC analyses were done on day 5 and compared among groups. (C) Tumors harvested on day 60 were analyzed by flow cytometry, and the frequencies of human CD45(+) or human CD8(+) tumor-infiltrating lymphocytes were compared among groups. (D) Immunohistochemical (IHC) staining of tumor sections by anti-human CD3 antibody (x10) on day 60 post-treatment. The number of T cells was compared among groups using Qpath analysis. (E) In vivo anti-tumor effect of GD2-EATs with anti-Ly6G or anti-GR1 antibody was tested against 143B osteosarcoma cell line xenografts. **Supplementary Fig. S5.** (A) Luciferase transduced T cells [Luc(+) T cells] or Luciferase transduced GD2-BsAb armed T cells [Luc(+) GD2-EATs] were administered with anti-Ly6G antibody to the mice bearing neuroblastoma patient-derived xenograft (PDX). (B) Bioluminescence in the lesions of the tumor was monitored. The bioluminescence images on day 8 and quantification of the bioluminescence in the lesions of the tumor. **Supplementary Fig. S6.** (A) Osteosarcoma cell line xenografts were treated by GD2-BsAb armed T cells (GD2-EATs) with anti-Ly6C antibodies. (B) CBC analyses were done on day 5 and compared among groups. (C) Tumors harvested on day 60 were analyzed by flow cytometry, and the frequencies of human CD45(+) or human CD8(+) tumor-infiltrating lymphocytes were compared among groups. (D) Immunohistochemical (IHC) staining of tumor sections by anti-human CD3 antibody (x10) on day 60 post-treatment. The number of T cells was compared among groups using Qpath analysis. (E) In vivo anti-tumor effect of GD2-EATs with anti-Ly6C antibody was tested against 143B osteosarcoma cell line xenografts. **Supplementary Fig. S7.** (A) Clodronate liposome (CL, 100µL) depleted macrophages in the liver. Livers were stained with immunofluorescence antibodies (green, murine CD68; blue, nuclei). (B) Anti-CSF1R antibody and 10µL of CL successfully depleted macrophages in the spleen. Spleens were processed with immunohistochemical (IHC) staining using murine CD68 antibody. (C) IHC staining of human CD3(+) T cells in 143B tumor sections after treatment with GD2-EATs plus anti-CSF1R antibody (x20). CD3(+) T cell number was compared with tumors treated with GD2-EATs alone. (D) IHC staining of human CD45(+) T cells in M14 tumor sections after treatment with T cells plus GD2-BsAb and CL (x10), and the number of CD45(+) T cells was compared. **Supplementary Fig. S8.** (A) Luciferase transduced T cells [Luc(+) T cells] were injected with clodronate liposome (CL) to small cell lung cancer (SCLC) cell line xenografts. The bioluminescence of Luc(+) T cell was monitored. The bioluminescence images on day 4 and quantification of the bioluminescence in the lesions of the tumor. (B) Luciferase transduced HER2-BsAb armed T cells [Luc(+) HER2-EATs] were administered with anti-CSF1R antibody to HER2(+)

osteosarcoma PDXs bearing mice. The bioluminescence of Luc(+) HER2-EATs was monitored. The bioluminescence images on day 4 and quantification of the bioluminescence in the lesions of the tumor. **Supplementary Fig. S9.** (A) In vivo anti-tumor effect of GD2-BsAb armed T cells (GD2-EATs) plus clodronate liposome (CL) was studied in 143B osteosarcoma cell line xenograft model. (B) The anti-tumor effect of GD2-EATs plus anti-CSF1R antibody was tested against osteosarcoma patient-derived xenografts (PDXs), and overall survival was analyzed. **Supplementary Fig. S10.** (A) Increasing doses of dexamethasone with GD2-BsAb armed T cells (GD2-EATs) were administered to mice bearing neuroblastoma patient-derived xenograft (PDX). TH1 cell cytokines were measured at different time points post-GD2-BsAb armed T cell (GD2-EAT) injection. (B) In vivo TH1 cell cytokine release was compared among groups. **Supplementary Fig. S11.** (A) Tumors were harvested on day 25 post-treatment and analyzed by flow cytometry. G-MDSC was gated as anti-mouse CD45+CD11b+Ly6G+; M-MDSC was gated as anti-mouse CD45+CD11b+Ly6G-Ly6Chi; TAM was gated as anti-mouse CD45+CD11b+Ly6G-Ly6CloF4/80+; Ly6Clo MDSC was gated as anti-mouse CD45+CD11b+Ly6G-Ly6CloF4/80-. G1, no treatment; G2, unarmed T cells; G3, unarmed T cells plus high-dose (HD) dexamethasone; G4, GD2-EATs; G5, GD2-EATs plus low-dose (LD) dexamethasone; G6, GD2-EATs plus intermediate-dose (ID) dexamethasone; G7, GD2-EATs plus high-dose (HD) dexamethasone. **Supplementary Fig. S12.** (A) Luciferase transduced T cells [Luc(+) T cells] or Luciferase transduced GD2-BsAb armed T cells [Luc(+) GD2-EATs] were administered with increasing doses of dexamethasone to the mice bearing osteosarcoma patient-derived xenograft (PDX). (B) Bioluminescence in the lungs and in the lesions of the tumor was monitored. The bioluminescence images in the lungs on day 1 and in the lesions of tumor on day 5 and quantification of the bioluminescence in the lesions of the tumor. **Supplementary Fig. S13.** (A) In vivo anti-tumor effect of dexamethasone premedication on GD2-BsAb directed T cell immunotherapy. 1x10⁷ of T cells and 5µg of GD2-BsAb were administered with increasing doses of dexamethasone to mice bearing neuroblastoma patient-derived xenograft (PDX). (B) Increasing doses of dexamethasone with GD2-BsAb armed T cells (GD2-EATs) were administered to treat osteosarcoma PDXs. Tumor growth, body weight change, and overall survival were analyzed.

Acknowledgements

We would like to especially thanks to Drs. Irene Cheung, Alan W. Long and Madelyn Epinosa-Cotton for their valuable comments during the preparation of this manuscript, and Dr. Elisa de Stanchina for her expertise in the establishment and maintenance of the PDXs.

Authors' contributions

JP, LW and N-KV. Cheung designed the experiments, interpreted, and analyzed the results and wrote the manuscript. All authors reviewed this manuscript and approved final the manuscript.

Funding

This work was supported in part by funds from Enid A. Haupt Endowed Chair, the Robert Steel Foundation, Kids Walk for Kids with Cancer. Technical service provided by the MSK Animal Imaging Core Facility, Antitumor Assessment Core Facility, and Molecular Cytology Core Facility were supported in part by the NCI Cancer Center Support Grant P30 CA008748.

Availability of data and materials

All data generated or analyzed during this study are included in this published article or uploaded as supplementary information.

Declarations

Ethics approval

All animal experiments were approved by the Memorial Sloan Kettering's Institutional Animal Care and Use Committee (IACUC) and were executed according to the ACUC guidelines. Patient-derived tumor xenografts were established with MSKCC IRB approval.

Consent for publication

Not applicable.

Competing interests

NKC reports past commercial research grants from Y-mAbs Therapeutics for hu3F8, 8H9, bispecific antibodies for CD33 and GD2, and a grant for SADA technology transfer; NKC has ownership interest/equity in Y-mAbs Therapeutics Inc., Abpro-Labs, and Eureka Therapeutics. NKC is the inventor and owner of issued patents licensed by MSK to Y-mAbs Therapeutics, Biotec Pharmacon, and Abpro-labs. Hu3F8, 8H9, bispecific antibodies against CD33 and GD2 were licensed by MSK to Y-mAbs Therapeutics. NKC is an advisory board member of Eureka Therapeutics. MSK has financial interest in Y-mabs. JP has no disclosures to report.

Received: 24 June 2021 Accepted: 30 August 2021

Published online: 08 September 2021

References

- Zhang Z, Liu S, Zhang B, Qiao L, Zhang Y. T cell dysfunction and exhaustion in cancer. *Front Cell Dev Biol.* 2020;8:17.
- Polyak K, Haviv I, Campbell IG. Co-evolution of tumor cells and their microenvironment. *Trends Genet.* 2009;25(1):30–8.
- Petrova V, Annicchiarico-Petruzzelli M, Melino G, Amelio I. The hypoxic tumour microenvironment. *Oncogenesis.* 2018;7(1):10.
- Gabrilovich DI, Nagaraj S. Myeloid-derived suppressor cells as regulators of the immune system. *Nat Rev Immunol.* 2009;9(3):162–74.
- Murdoch C, Muthana M, Coffelt SB, Lewis CE. The role of myeloid cells in the promotion of tumour angiogenesis. *Nat Rev Cancer.* 2008;8(8):618–31.
- Langsten KL, Kim JH, Sarver AL, Dewhurst M, Modiano JF. Comparative approach to the temporo-spatial organization of the tumor microenvironment. *Front Oncol.* 2019;9:1185.
- Zhao Y, Dong Q, Li J, Zhang K, Qin J, Zhao J, Sun Q, Wang Z, Wartmann T, Jauch KW, et al. Targeting cancer stem cells and their niche: perspectives for future therapeutic targets and strategies. *Semin Cancer Biol.* 2018;53:139–55.
- Aponte PM, Caicedo A. Stemness in cancer: stem cells, cancer stem cells, and their microenvironment. *Stem Cells Int.* 2017;2017:5619472.
- Movahedi K, Guillems M, Van den Bossche J, Van den Bergh R, Gysemans C, Beschin A, De Baetselier P, Van Ginderachter JA. Identification of discrete tumor-induced myeloid-derived suppressor cell subpopulations with distinct T cell-suppressive activity. *Blood.* 2008;111(8):4233–44.
- Youn JI, Nagaraj S, Collazo M, Gabrilovich DI. Subsets of myeloid-derived suppressor cells in tumor-bearing mice. *J Immunol.* 2008;181(8):5791–802.
- Fleming TJ, Fleming ML, Malek TR. Selective expression of Ly-6G on myeloid lineage cells in mouse bone marrow. RB6–8C5 mAb to granulocyte-differentiation antigen (Gr-1) detects members of the Ly-6 family. *J Immunol.* 1993;151(5):2399–408.
- Sunderkötter C, Nikolic T, Dillon MJ, Van Rooijen N, Stehling M, Drevets DA, Leenen PJ. Subpopulations of mouse blood monocytes differ in maturation stage and inflammatory response. *J Immunol.* 2004;172(7):4410–7.
- Cassetta L, Noy R, Swierczak A, Sugano G, Smith H, Wiechmann L, Pollard JW. Isolation of mouse and human tumor-associated macrophages. *Adv Exp Med Biol.* 2016;899:211–29.
- Bronte V, Brandau S, Chen SH, Colombo MP, Frey AB, Greten TF, Mandruzzato S, Murray PJ, Ochoa A, Ostrand-Rosenberg S, et al. Recommendations for myeloid-derived suppressor cell nomenclature and characterization standards. *Nat Commun.* 2016;7:12150.
- Yu J, Du W, Yan F, Wang Y, Li H, Cao S, Yu W, Shen C, Liu J, Ren X. Myeloid-derived suppressor cells suppress antitumor immune responses through IDO expression and correlate with lymph node metastasis in patients with breast cancer. *J Immunol.* 2013;190(7):3783–97.
- Srivastava MK, Sinha P, Clements VK, Rodriguez P, Ostrand-Rosenberg S. Myeloid-derived suppressor cells inhibit T-cell activation by depleting cystine and cysteine. *Cancer Res.* 2010;70(1):68–77.
- Hammami A, Allard D, Allard B, Stagg J. Targeting the adenosine pathway for cancer immunotherapy. *Semin Immunol.* 2019;42:101304.
- Hanson EM, Clements VK, Sinha P, Ilkovich D, Ostrand-Rosenberg S. Myeloid-derived suppressor cells down-regulate L-selectin expression on CD4+ and CD8+ T cells. *J Immunol.* 2009;183(2):937–44.
- Noman MZ, Desantis G, Janji B, Hasmim M, Karray S, Dessen P, Bronte V, Chouaib S. PD-L1 is a novel direct target of HIF-1 α , and its blockade under hypoxia enhanced MDSC-mediated T cell activation. *J Exp Med.* 2014;211(5):781–90.
- Noy R, Pollard JW. Tumor-associated macrophages: from mechanisms to therapy. *Immunity.* 2014;41(1):49–61.
- Park JA, Cheung NV. GD2 or HER2 targeting T cell engaging bispecific antibodies to treat osteosarcoma. *J Hematol Oncol.* 2020;13(1):172.
- Xu H, Cheng M, Guo H, Chen Y, Huse M, Cheung NK. Retargeting T cells to GD2 pentasaccharide on human tumors using Bispecific humanized antibody. *Cancer Immunol Res.* 2015;3(3):266–77.
- Orcutt KD, Ackerman ME, Cieslewicz M, Quiroz E, Slusarczyk AL, Frangioni JV, Wittrup KD. A modular IgG-scFv bispecific antibody topology. *Prot Eng Des Sel.* 2010;23(4):221–8.
- Reikofski J, Tao BY. Polymerase chain reaction (PCR) techniques for site-directed mutagenesis. *Biotechnol Adv.* 1992;10(4):535–47.
- Park JA, Santich BH, Xu H, Lum LG, Cheung NV. Potent ex vivo armed T cells using recombinant bispecific antibodies for adoptive immunotherapy with reduced cytokine release. *J Immunother Cancer.* 2021;9(5).
- Dunn WD Jr, Gearing M, Park Y, Zhang L, Hanfelt J, Glass JD, Gutman DA. Applicability of digital analysis and imaging technology in neuropathology assessment. *Neuropathology.* 2016;36(3):270–82.
- Nair AB, Jacob S. A simple practice guide for dose conversion between animals and human. *J Basic Clin Pharm.* 2016;7(2):27–31.
- Santich BH, Park JA, Tran H, Guo HF, Huse M, Cheung NV. Interdomain spacing and spatial configuration drive the potency of IgG-[L]-scFv T cell bispecific antibodies. *Sci Transl Med.* 2020;12(534).
- Lopez-Albaitero A, Xu H, Guo H, Wang L, Wu Z, Tran H, Chandrapaty S, Scaltriti M, Janjigian Y, de Stanchina E, et al. Overcoming resistance to HER2-targeted therapy with a novel HER2/CD3 bispecific antibody. *Oncoimmunology.* 2017;6(3):e1267891.
- Park JA, Santich BH, Xu H, Lum LG, Cheung N-KV. Potent ex vivo armed T cells using recombinant bispecific antibodies for adoptive immunotherapy with reduced cytokine release. *J Immunother Cancer.* 2021;9(5):e00222.
- Coussens LM, Zitvogel L, Palucka AK. Neutralizing tumor-promoting chronic inflammation: A magic bullet? *Science.* 2013;339(6117):286–91.
- Ruffell B, Chang-Strachan D, Chan V, Rosenbusch A, Ho CM, Pryer N, Daniel D, Hwang ES, Rugo HS, Coussens LM. Macrophage IL-10 blocks CD8+ T cell-dependent responses to chemotherapy by suppressing IL-12 expression in intratumoral dendritic cells. *Cancer Cell.* 2014;26(5):623–37.
- Qian BZ, Pollard JW. Macrophage diversity enhances tumor progression and metastasis. *Cell.* 2010;141(1):39–51.
- Jung M, Mertens C, Tomat E, Brüne B. Iron as a central player and promising target in cancer progression. *Int J Mol Sci.* 2019;20(2).
- Wang W, Green M, Choi JE, Gijon M, Kennedy PD, Johnson JK, Liao P, Lang X, Kryczek I, Sell A et al. CD8. *Nature.* 2019;569(7755):270–274.
- Stockwell BR, Jiang X. A physiological function for ferroptosis in tumor suppression by the immune system. *Cell Metab.* 2019;30(1):14–5.
- Dai E, Han L, Liu J, Xie Y, Kroemer G, Klionsky DJ, Zeh HJ, Kang R, Wang J, Tang D. Autophagy-dependent ferroptosis drives tumor-associated macrophage polarization via release and uptake of oncogenic KRAS protein. *Autophagy.* 2020;16(11):2069–83.
- Wu Y, Yu C, Luo M, Cen C, Qiu J, Zhang S, Hu K. Ferroptosis in cancer treatment: another way to Rome. *Front Oncol.* 2020;10:571127.
- Wang H, An P, Xie E, Wu Q, Fang X, Gao H, Zhang Z, Li Y, Wang X, Zhang J, et al. Characterization of ferroptosis in murine models of hemochromatosis. *Hepatology.* 2017;66(2):449–65.
- Kapralov AA, Yang Q, Dar HH, Tyurina YY, Anthonymuthu TS, Kim R, St Croix CM, Mikulska-Ruminska K, Liu B, Shrivastava IH, et al. Redox lipid reprogramming commands susceptibility of macrophages and microglia to ferroptotic death. *Nat Chem Biol.* 2020;16(3):278–90.
- MacDonald KP, Palmer JS, Cronau S, Seppanen E, Olver S, Raffelt NC, Kuns R, Pettit AR, Clouston A, Wainwright B, et al. An antibody against the colony-stimulating factor 1 receptor depletes the resident subset of monocytes and tissue- and tumor-associated macrophages but does not inhibit inflammation. *Blood.* 2010;116(19):3955–63.

42. Arbour KC, Mezquita L, Long N, Rizvi H, Auclin E, Ni A, Martinez-Bernal G, Ferrara R, Lai WW, Hendriks LEL, et al. Impact of baseline steroids on efficacy of programmed cell death-1 and programmed death-ligand 1 blockade in patients with non-small-cell lung cancer. *J Clin Oncol*. 2018;36(28):2872–8.
43. Jove M, Vilarino N, Nadal E. Impact of baseline steroids on efficacy of programmed cell death-1 (PD-1) and programmed death-ligand 1 (PD-L1) blockade in patients with advanced non-small cell lung cancer. *Transl Lung Cancer Res*. 2019;8(Suppl 4):S364–8.
44. Brandl C, Haas C, d'Argouges S, Fisch T, Kufer P, Brischwein K, Prang N, Bargou R, Suzich J, Baeuerle PA, et al. The effect of dexamethasone on polyclonal T cell activation and redirected target cell lysis as induced by a CD19/CD3-bispecific single-chain antibody construct. *Cancer Immunol Immunother*. 2007;56(10):1551–63.
45. Viardot A, Goebeler ME, Hess G, Neumann S, Pfreundschuh M, Adrian N, Zettl F, Libicher M, Sayehli C, Stiegmaier J, et al. Phase 2 study of the bispecific T-cell engager (BiTE) antibody blinatumomab in relapsed/refractory diffuse large B-cell lymphoma. *Blood*. 2016;127(11):1410–6.
46. Kanai T, Seki S, Jenks JA, Kohli A, Kawli T, Martin DP, Snyder M, Bacchetta R, Nadeau KC. Identification of STAT5A and STAT5B target genes in human T cells. *PLoS ONE*. 2014;9(1):e86790.
47. Meyer LK, Verbist KC, Albeituni S, Scull BP, Bassett RC, Stroh AN, Tillman H, Allen CE, Hermiston ML, Nichols KE. JAK/STAT pathway inhibition sensitizes CD8 T cells to dexamethasone-induced apoptosis in hyperinflammation. *Blood*. 2020;136(6):657–68.
48. Lim HY, Muller N, Herold MJ, van den Brandt J, Reichardt HM. Glucocorticoids exert opposing effects on macrophage function dependent on their concentration. *Immunology*. 2007;122(1):47–53.
49. Berrebi D, Bruscoli S, Cohen N, Foussat A, Migliorati G, Bouchet-Delbos L, Maillot MC, Portier A, Couderc J, Galanaud P, et al. Synthesis of glucocorticoid-induced leucine zipper (GILZ) by macrophages: an anti-inflammatory and immunosuppressive mechanism shared by glucocorticoids and IL-10. *Blood*. 2003;101(2):729–38.
50. Gerke V, Creutz CE, Moss SE. Annexins: linking Ca²⁺ signalling to membrane dynamics. *Nat Rev Mol Cell Biol*. 2005;6(6):449–61.
51. Perretti M, D'Acquisto F. Annexin A1 and glucocorticoids as effectors of the resolution of inflammation. *Nat Rev Immunol*. 2009;9(1):62–70.
52. Maderna P, Yona S, Perretti M, Godson C. Modulation of phagocytosis of apoptotic neutrophils by supernatant from dexamethasone-treated macrophages and annexin-derived peptide Ac(2–26). *J Immunol*. 2005;174(6):3727–33.
53. Uhlenhaut NH, Barish GD, Yu RT, Downes M, Karunasiri M, Liddle C, Schwalie P, Hubner N, Evans RM. Insights into negative regulation by the glucocorticoid receptor from genome-wide profiling of inflammatory cistromes. *Mol Cell*. 2013;49(1):158–71.
54. Desgeorges T, Caratti G, Mounier R, Tuckermann J, Chazaud B. Glucocorticoids shape macrophage phenotype for tissue repair. *Front Immunol*. 2019;10:1591.
55. Chen J, Lopez-Moyado IF, Seo H, Lio CJ, Hempleman LJ, Sekiya T, Yoshimura A, Scott-Browne JP, Rao A. NR4A transcription factors limit CAR T cell function in solid tumours. *Nature*. 2019;567(7749):530–4.
56. Chen J, Ye Y, Liu P, Yu W, Wei F, Li H, Yu J. Suppression of T cells by myeloid-derived suppressor cells in cancer. *Hum Immunol*. 2017;78(2):113–9.
57. Li C, Jiang P, Wei S, Xu X, Wang J. Regulatory T cells in tumor microenvironment: new mechanisms, potential therapeutic strategies and future prospects. *Mol Cancer*. 2020;19(1):116.
58. Jung K, Heishi T, Khan OF, Kowalski PS, Incio J, Rahbari NN, Chung E, Clark JW, Willett CG, Luster AD, et al. Ly6Clo monocytes drive immunosuppression and confer resistance to anti-VEGFR2 cancer therapy. *J Clin Invest*. 2017;127(8):3039–51.
59. McKee SJ, Tuong ZK, Kobayashi T, Doff BL, Soon MS, Nissen M, Lam PY, Keane C, Vari F, Moi D, et al. B cell lymphoma progression promotes the accumulation of circulating Ly6Clo monocytes with immunosuppressive activity. *Oncoimmunology*. 2018;7(2):e1393599.
60. Netherby CS, Messmer MN, Burkard-Mandel L, Colligan S, Miller A, Cortes Gomez E, Wang J, Nemeth MJ, Abrams SI. The granulocyte progenitor stage is a key target of IRF8-mediated regulation of myeloid-derived suppressor cell production. *J Immunol*. 2017;198(10):4129–39.
61. Condamine T, Mastio J, Gabrilovich DI. Transcriptional regulation of myeloid-derived suppressor cells. *J Leukoc Biol*. 2015;98(6):913–22.
62. Qin H, Lerman B, Sakamaki I, Wei G, Cha SC, Rao SS, Qian J, Hailemichael Y, Nurieva R, Dwyer KC, et al. Generation of a new therapeutic peptide that depletes myeloid-derived suppressor cells in tumor-bearing mice. *Nat Med*. 2014;20(6):676–81.
63. Ibanez-Vea M, Zuazo M, Gato M, Arasanz H, Fernandez-Hinojal G, Escors D, Kochan G. Myeloid-derived suppressor cells in the tumor microenvironment: current knowledge and future perspectives. *Arch Immunol Ther Exp (Warsz)*. 2018;66(2):113–23.
64. Netherby CS, Abrams SI. Mechanisms overseeing myeloid-derived suppressor cell production in neoplastic disease. *Cancer Immunol Immunother*. 2017;66(8):989–96.
65. Zilionis R, Engblom C, Pfirschke C, Savova V, Zemmour D, Saatcioglu HD, Krishnan I, Maroni G, Meyerovitz CV, Kerwin CM et al. Single-cell transcriptomics of human and mouse lung cancers reveals conserved myeloid populations across individuals and species. *Immunity* 2019; 50(5):1317–1334 e1310.
66. Weinberg RA: Is metastasis predetermined? *Mol Oncol* 2007;1(3):263–264; author reply 265–266.
67. Walrath JC, Hawes JJ, Van Dyke T, Reilly KM. Genetically engineered mouse models in cancer research. *Adv Cancer Res*. 2010;106:113–64.

Publisher's Note

Springer Nature remains neutral with regard to jurisdictional claims in published maps and institutional affiliations.

Ready to submit your research? Choose BMC and benefit from:

- fast, convenient online submission
- thorough peer review by experienced researchers in your field
- rapid publication on acceptance
- support for research data, including large and complex data types
- gold Open Access which fosters wider collaboration and increased citations
- maximum visibility for your research: over 100M website views per year

At BMC, research is always in progress.

Learn more biomedcentral.com/submissions

